Electronic Transactions on Numerical Analysis.
Volume 44, pp. 497–521, 2015.

ISSN 1068–9613.

ETNA
Kent State University
http://etna.math.kent.edu

A TWO-LEVEL OVERLAPPING SCHWARZ METHOD FOR H(CURL) IN TWO DIMENSIONS WITH IRREGULAR SUBDOMAINS*

JUAN G. CALVO†

Abstract. A bound is obtained for the condition number of a two-level overlapping Schwarz algorithm for problems posed in $H(\mathrm{curl})$ in two dimensions, where the subdomains are only assumed to be John subdomains. The coarse space is based on energy minimization and its dimension equals the number of interior subdomain edges. Local direct solvers are used on the overlapping subdomains. Our bound depends only on a few geometric parameters of the decomposition. This bound is independent of jumps in the coefficients across the interface between the subdomains for most of the different cases considered. Numerical experiments that verify the result are shown, including some with subdomains with fractal edges and others obtained by a mesh partitioner.

Key words. Domain decomposition, overlapping Schwarz algorithms, preconditioners, irregular subdomain boundaries, H(curl), Maxwell's equations, discontinuous coefficients

AMS subject classifications. 65N55, 65N30, 65F10, 35Q60

1. Introduction.

We consider the boundary value problem in two dimensions (2D)

$$\begin{aligned} \nabla \times (\alpha \nabla \times \boldsymbol{u}) + B\boldsymbol{u} &= \boldsymbol{f} \quad \text{in } \Omega, \\ \boldsymbol{u} \times \boldsymbol{n} &= 0 \quad \text{on } \partial\Omega, \end{aligned} \tag{1.1}$$

where $\alpha(\boldsymbol{x}) \geq 0$, and B is a 2×2 strictly positive definite symmetric matrix. We could equally well consider cases where the boundary condition is imposed only on one or several subdomain edges which form part of $\partial\Omega$, imposing a natural boundary condition over the rest of the boundary.

In order to formulate an appropriate weak form for this problem, we consider the Hilbert space $H(\mathrm{curl}, \Omega)$, the subspace of $(L^2(\Omega))^2$ with a curl with a finite L^2-norm. We then obtain a weak formulation for (1.1): find $\boldsymbol{u} \in H_0(\mathrm{curl}, \Omega)$ such that

$$a(\boldsymbol{u}, \boldsymbol{v}) = (\boldsymbol{f}, \boldsymbol{v}) \; \forall \boldsymbol{v} \in H_0(\mathrm{curl}, \Omega), \tag{1.2}$$

with

$$a(\boldsymbol{u}, \boldsymbol{v}) := \int_\Omega \left[\alpha(\nabla \times \boldsymbol{u})(\nabla \times \boldsymbol{v}) + B\boldsymbol{u} \cdot \boldsymbol{v}\right] d\boldsymbol{x}, \qquad (\boldsymbol{f}, \boldsymbol{v}) := \int_\Omega \boldsymbol{f} \cdot \boldsymbol{v} d\boldsymbol{x}. \tag{1.3}$$

Here, $H_0(\mathrm{curl}, \Omega)$ is the subspace of $H(\mathrm{curl}, \Omega)$ with a vanishing tangential component on $\partial\Omega$. For a scalar function p and a vector-valued function $\boldsymbol{u}$, the vector and scalar curl operators are defined, respectively, by $\nabla \times p = (\partial_{x_2} p, -\partial_{x_1} p)^T$ and $\nabla \times \boldsymbol{u} = \partial_{x_1} u_2 - \partial_{x_2} u_1$. The norm of $\boldsymbol{u} \in H(\mathrm{curl}, \Omega)$, for a domain with diameter 1, is given by $a(\boldsymbol{u}, \boldsymbol{u})^{1/2}$ with $\alpha = 1$ and $B = I$. The problem (1.2) arises, for example, from implicit time integration of the eddy current model of Maxwell's equation; see [3, Chapter 8]. It is also considered in [1, 14, 27, 32].

We decompose the domain Ω into N non-overlapping subdomains $\{\Omega_i\}_{i=1}^N$, which are John domains [15] and each of which is the union of elements of the triangulation $\mathcal{T}_h$ of Ω. Each Ω_i is simply connected and has a connected boundary $\partial\Omega_i$. We denote by H_i the diameter of Ω_i and by h_i the smallest element diameter of the shape-regular triangulation $\mathcal{T}_{h_i}$

*Received November 10, 2014. Accepted June 11, 2015. Published online on October 7, 2015. Recommended by Jing Li. This work was supported in part by the National Science Foundation Grant DMS-1216564 and in part by the U.S. Department of Energy under contracts DE-FG02-06ER25718.

†CIMPA, Universidad de Costa Rica, San Jose, Costa Rica, 11501 (juan.calvo@ucr.ac.cr).

ETNA
Kent State University
http://etna.math.kent.edu

of Ω_i. We define $H/h := \max H_i/h_i$, $H/\delta := \max H_i/\delta_i$ and $\delta/h := \max \delta_i/h_i$. Here δ_i measures the overlap between overlapping subdomains; see Section 2 for the formal definition.

The main purpose of this paper is to construct and analyze a two-level overlapping Schwarz method for the problem (1.2) discretized with Nédélec finite elements (introduced in [21]) in two dimensions and for irregular subdomains. The condition number estimate will be given in terms of a few simple geometric parameters of the subdomains Ω_i. This study is part of the analysis of the most current important domain decomposition techniques for our problem with irregular subdomains in 2D, since an iterative substructuring algorithm is analyzed in [10], and a Balancing Domain Decomposition by Constraints (BDDC) deluxe method is considered in [5]. We recall that the dual-primal finite element tearing and interconnecting (FETI-DP) methods are closely related to the BDDC methods.

Our study is based on [10], where an iterative substructuring algorithm is introduced for two-dimensional problems in the space $H_0(\mathrm{curl}, \Omega)$. Our coarse space is based on energy minimization and its dimension equals the number of interior subdomain edges (see end of Section 2). In the present study, we borrow the coarse space and modify some of the results from [10]; that paper also reports on some numerical experiments with an overlapping Schwarz algorithm very similar to ours.

We introduce a new type of cutoff function for overlapping regions with John subdomains. We note that certain snowflake curves with fractal boundaries are John domains, and that the length of the boundary of a John domain can be arbitrary larger that its diameter. This cutoff function allows us to define local decompositions, and can be used in different overlapping Scharwz algorithms for problems with discontinuities in the coefficients across the interface, reducing the problem to obtaining local bounds. This idea is used in Section 5.1, where we analyze a stability result for our coarse space.

In domain decomposition theory, it is typically assumed that each subdomain is quite regular; e.g., the union of a small set of coarse triangles or tetrahedra. But, it is unrealistic in general to assume that each subdomain is regular. Thus, subdomain boundaries that arise from mesh partitioners might not even be Lipschitz continuous, i.e., the number of patches required to cover the boundary of the region in each of which the boundary is the graph of a Lipschitz continuous function, might not be uniformly bounded independently of the finite element mesh size. Some recent work and technical tools have been developed for irregular subdomains, surveyed in [33]. Scalar elliptic problems in the plane are analyzed in [7, 9]; [17] includes a FETI-DP algorithm for scalar elliptic and elasticity problems, and [5, 10] include an iterative substructuring method and a BDDC deluxe algorithm for problems in $H(\mathrm{curl})$ in 2D, respectively.

The standard way of constructing the local components involves a partition of unity for all of Ω. This is a decomposition of functions in the sense of the Schwarz theory as in [31, Chapter 2]. In our study, we adopt a different strategy, creating a partition of unity for the interface and we then split the corresponding functions supported in the different overlapping regions, in a way similar to what is done in [8].

In a previous study related to $H(\mathrm{curl})$, the estimate $\kappa \leq C(1 + H/\delta)^2$ is given in [27] for an overlapping Schwarz algorithm in three dimensions, where the coarse space consists of standard edge finite element functions for coarse tetrahedral elements, the domain is assumed convex and $\alpha \equiv 1$, $B \equiv I$ over the whole domain. The coarse triangulation is shape-regular and quasi-uniform.

Work on vector-valued problems include [13], where overlapping Schwarz methods are analyzed for elliptic problems in $H(\mathrm{curl})$ and $H(\mathrm{div})$ in three dimensions. With the assumption of a convex polyhedral domain and $B = I$, the condition number is bounded by $C(1 + H/\delta)^2$, where subdomains are tetrahedra and constant coefficients are considered.

ETNA
Kent State University
http://etna.math.kent.edu

Also in [32, 34], the bound $C(1+\log(H/h))^2$ is found for $H(\mathrm{div})$ and $H(\mathrm{curl})$ problems for bounded polygonal domains in $\mathbb{R}^3$ and $\mathbb{R}^2$ respectively, where an iterative substructuring algorithm is used with shape regular hexahedral and triangular subdomains. In [22], a two-level overlapping Schwarz method for Raviart-Thomas vector fields is developed. Here the bilinear form is

$$a(\boldsymbol{u},\boldsymbol{v}) = \int_\Omega [\alpha \mathrm{div}\, \boldsymbol{u}\ \mathrm{div}\, \boldsymbol{v} + B\boldsymbol{u}\cdot\boldsymbol{v}]d\boldsymbol{x}$$

and the condition number is bounded by $C(1+H/\delta)(1+\log(H/h))$, where the domain is a bounded polyhedron in $\mathbb{R}^3$ and discontinuous coefficients and hexahedral elements are considered. Studies based on FETI algorithms for our problem include [29, 30] for problems posed in 2D, and [28] in 3D. The subdomains are bounded convex polyhedra and the bounds depend on the coefficients α_i, β_i and H_i. In addition, a BDDC algorithm with deluxe scaling is considered in [5] for uniform domains in 2D, and in [11] for 3D. A deluxe FETI-DP algorithm for a hybrid staggered discontinuous Galerkin method for H(curl) is analyzed in [6].

There are also some related studies with Algebraic Multigrid Methods (AMG). In [18], a parallel implementation of different preconditioners based on the Hiptmair-Xu decomposition derived in [14] is analyzed. Also, different coarse spaces are constructed for problems in 3D and unstructed meshes in [19].

Our study applies to a much broader range of material properties and subdomain geometries than previous studies. We obtain the bound

$$\kappa \leq C|\Xi|\chi\eta\left(1+\log\frac{\delta}{h}\right)\left(1+\frac{H}{\delta}\right)\left(1+\log\frac{H}{h}\right),$$

where C is independent of the jumps of the coefficients between the subdomains and the number of subdomains. The parameter χ is related to the geometry of the subdomains and it is quite close to 1 even for fractal edges and large values of H/h (see Section 2), $|\Xi|$ represents the maximum number of neighbors for any subdomain, and

$$\eta = \max_i \left\{1+\frac{\beta_i H_i^2}{\alpha_i}\right\},$$

where the maximum is taken over all the subdomains; see Section 5.1. We observe that in many cases we can obtain a bound independent of the coefficients; see Theorem 5.2 and Remark 5.4. Also, for a small overlap, we note that the factor $(1+\log(\delta/h))$ is not significant in our estimate.

The rest of this paper is organized as follows. In Section 2, we introduce the notation used. In Section 3, we recall the definition of John domains and provide some related lemmas. In Section 4, we present some technical tools that are used to prove our estimate of the condition number in Section 5. In Section 6, we report on some numerical experiments, which confirm our theoretical result.

2. Notation. We introduce some notation that we will use throughout this paper. The interface of the decomposition $\{\Omega_i\}_{i=1}^N$ is given by

$$\Gamma := \left(\bigcup_{i=1}^N \partial\Omega_i\right) \setminus \partial\Omega,$$

and the contribution to Γ from $\partial\Omega_i$ by $\Gamma_i := \partial\Omega_i \setminus \partial\Omega$. These sets are unions of subdomain edges and vertices. We denote the subdomain edges of $\partial\Omega_i$ by $\mathcal{E}^{ij} := \overline{\Omega}_i \cap \overline{\Omega}_j$, excluding the

ETNA
Kent State University
http://etna.math.kent.edu

two vertices at their endpoints. We note that the intersection of the closure of two subdomains might have several components. In such a case, each component will be regarded as an edge. We will write $\mathcal{E}$ instead of $\mathcal{E}^{ij}$ when there is no ambiguity.

The set of all subdomain edges is defined as

$$S_{\mathcal{E}} := \{\mathcal{E}^{ij} : i < j, \mathcal{E}^{ij} \neq \emptyset\}$$

and $S_{\mathcal{E}_i}$ is the subset of subdomain edges which belong to Γ_i. When there is a need to uniquely define the unit tangential vector $\boldsymbol{t}_{\mathcal{E}}$ over a subdomain edge, we will select the subdomain with the smallest index and use the counterclock-wise direction over its boundary. The unit vector in the direction from one endpoint of a subdomain edge $\mathcal{E}$ to the other (with the same sense of direction as $\boldsymbol{t}_{\mathcal{E}}$) is denoted by $\boldsymbol{d}_{\mathcal{E}}$. The distance between the two endpoints is $d_{\mathcal{E}}$.

For any irregular subdomain edge, we will consider a covering by disks and we will denote by $\chi_{\mathcal{E}}(d)(d_{\mathcal{E}}/d)$ the number of closed circular disks of diameter d that are required to cover it. We note that $\chi_{\mathcal{E}}(d) = 1$ if the edge is straight and that it can be proved that for a prefractal Koch snowflake curve, which is a polygon with side length h_i and diameter H_i, $\chi_{\mathcal{E}}(h_i) \leq (H_i/h_i)^{\log(4/3)} < (H_i/h_i)^{1/8}$; see [10, Section 3.2]. This is not a large factor, being less than 10 even in the extreme case of $H_i/h_i = 10^8$.

Associated with the triangulation $\mathcal{T}_{h_i}$, we consider the space of continuous, piecewise linear triangular nodal elements $W^{h_i}_{\mathrm{grad}}(\Omega_i) \subset H(\mathrm{grad}, \Omega_i)$, and the space $W^{h_i}_{\mathrm{curl}}(\Omega_i) \subset H(\mathrm{curl}, \Omega_i)$, based on linear triangular Nédélec edge elements on Ω_i with zero tangential component on $\partial\Omega \cap \partial\Omega_i$; see [21].

The Nédélec elements are conforming in $H(\mathrm{curl}, \Omega)$ and those of lowest order are defined by

$$W^h_{\mathrm{curl}}(\Omega) := \{\boldsymbol{u} | \boldsymbol{u}_{|K} \in \mathcal{N}_1(K), K \in \mathcal{T}_h \text{ and } \boldsymbol{u} \in H(\mathrm{curl}, \Omega)\},$$

where any function in $\mathcal{N}_1(K)$ has the form $\boldsymbol{u}(x_1, x_2) = (a_1 + bx_2, a_2 - bx_1)^T$, with a_1, a_2, b real numbers. The degrees of freedom for an element $K \in \mathcal{T}_h$ are given by the average values of the tangential component over the edges of the element, i.e.,

$$\lambda_e(\boldsymbol{u}) := \frac{1}{|e|} \int_e \boldsymbol{u} \cdot \boldsymbol{t}_e ds, \tag{2.1}$$

with $e \in \partial K$ and $\boldsymbol{t}_e$ a unit vector in the direction of e. We recall that a function in $W^h_{\mathrm{curl}}(\Omega)$ has a continuous tangential component across all the fine edges; see e.g., [21].

We obtain an overlapping decomposition $\{\Omega_i'\}$ by adding layers of elements to Ω_i and denote by δ_i the minimal distance from any edge $\mathcal{E}^{ij} \subset \Gamma_i$ to $\partial\Omega_j'$.

We will replace B by βI, and assume that α, β are constants α_i, β_i in each subdomain Ω_i. Denote by $a_i(\boldsymbol{u}, \boldsymbol{v})$ and $a_i'(\boldsymbol{u}, \boldsymbol{v})$ the bilinear form $a(\cdot, \cdot)$ defined in (1.3) and restricted to the domains Ω_i and Ω_i' respectively.

Let $\boldsymbol{N}_e \in W^{h_i}_{\mathrm{curl}}(\Omega_i)$ denote the finite element shape function for an edge e of the finite element mesh $\mathcal{T}_{h_i}$. We assume that $\boldsymbol{N}_e$ is scaled such that $\boldsymbol{N}_e \cdot \boldsymbol{t}_e = 1$ along e. The edge finite element interpolant of a sufficiently smooth vector function $\boldsymbol{u} \in H(\mathrm{curl}, \Omega_i)$ is then defined as

$$\Pi^{h_i}(\boldsymbol{u}) := \sum_{e \in M^{h_i}} u_e \boldsymbol{N}_e, \; u_e := \frac{1}{|e|} \int_e \boldsymbol{u} \cdot \boldsymbol{t}_e ds,$$

where M^{h_i} is the set of element edges of $\overline{\Omega}_i$ and $|e|$ is the length of e. The nodal finite element interpolant of a sufficiently smooth $p \in H(\mathrm{grad}, \Omega_i)$ is defined as

$$I^{h_i}(p) := \sum_{\boldsymbol{v} \in \mathcal{N}^{h_i}} p(\boldsymbol{v}) \phi_{\boldsymbol{v}}, \tag{2.2}$$

ETNA
Kent State University
http://etna.math.kent.edu

where $\mathcal{N}^{h_i}$ is the set of nodes of $\mathcal{T}_{h_i}$, $p(\boldsymbol{v})$ is the value of p at node $\boldsymbol{v}$, and $\phi_{\boldsymbol{v}} \in W^{h_i}_{\text{grad}}(\Omega_i)$ is the shape function for node $\boldsymbol{v}$.

We will consider the same coarse space functions as introduced in [10]. For $\mathcal{E} \in S_{\mathcal{E}}$, we define the coarse function $\boldsymbol{c}_{\mathcal{E}}$ with tangential data given by $\boldsymbol{c}_{\mathcal{E}} \cdot \boldsymbol{t}_e = \boldsymbol{d}_{\mathcal{E}} \cdot \boldsymbol{t}_e$ along $\mathcal{E}$ and with $\boldsymbol{c}_{\mathcal{E}} \cdot \boldsymbol{t}_e = 0$ on $\Gamma \cup \partial\Omega \setminus \mathcal{E}$. We obtain $\boldsymbol{c}_{\mathcal{E}}$ by the energy minimizing extension of this tangential data into the interior of the two subdomains sharing $\mathcal{E}$. We note that the construction of $\boldsymbol{c}_{\mathcal{E}^{ij}}$ involves the solution of a Dirichlet problem with inhomogeneous boundary data for Ω_i and Ω_j. We then define the coarse interpolant for $\boldsymbol{u} \in H(\text{curl}, \Omega)$ by

$$\boldsymbol{u_0} := \sum_{\mathcal{E} \in S_{\mathcal{E}}} \overline{u}_{\mathcal{E}} \boldsymbol{c}_{\boldsymbol{\mathcal{E}}}, \text{ with } \overline{u}_{\mathcal{E}} := \frac{1}{d_{\mathcal{E}}} \int_{\mathcal{E}} \boldsymbol{u} \cdot \boldsymbol{t}_{\mathcal{E}} ds. \tag{2.3}$$

3. John domains. We start by defining John domains and present some known theorems related to these domains. John domains where first considered by F. John in his work on elasticity [15].

DEFINITION 3.1 (John domain). *A domain $\Omega \subset \mathbb{R}^n$ — an open, bounded, and connected set — is a John domain if there exists a constant $C_J \geq 1$ and a distinguished central point $\boldsymbol{x}_0 \in \Omega$, such that each $\boldsymbol{x} \in \Omega$ can be joined to $\boldsymbol{x}_0$ by a rectifiable curve $\gamma : [0, 1] \to \Omega$, with $\gamma(0) = \boldsymbol{x}_0$, $\gamma(1) = \boldsymbol{x}$, and*

$$|\boldsymbol{x} - \gamma(t)| \leq C_J \cdot \text{dist}\left(\gamma(t), \partial\Omega\right), \ \forall t \in [0, 1].$$

REMARK 3.2. For a rectangular domain, $C_J \geq L_1/L_2$, where L_1, L_2 are the height and width of the domain, respectively. Thus, the constant C_J can be large if the subdomain has a large aspect ratio.

We have the following result; see [12, 20].

LEMMA 3.3 (Isoperimetric inequality). *Let $\Omega \subset \mathbb{R}^n$ be a domain, and let u be sufficiently smooth. Then,*

$$\inf_{c \in \mathbb{R}} \left(\int_{\Omega} |u - c|^{n/(n-1)} dx \right)^{(n-1)/n} \leq \gamma(\Omega, n) \int_{\Omega} |\nabla u| dx, \tag{3.1}$$

if and only if,

$$\left(\min\left(|A|, |B|\right)\right)^{1-1/n} \leq \gamma(\Omega, n) |\partial A \cap \partial B|.$$

Here, $A \subset \Omega$ is an arbitrary open set, and $B = \Omega \setminus \overline{A}$; $\gamma(\Omega, n)$ the best possible constant and $|A|$ the measure of the set A, etc.

A simply connected plane domain of finite area satisfies (3.1) if and only if Ω is a John domain; see [4]. Furthermore, the parameter $\gamma(\Omega, 2)$ can be expressed in terms of the John constant C_J; see [2]. For two dimensions, we immediately obtain a standard Poincaré inequality from (3.1) by using the Cauchy-Schwarz inequality. We note that the best choice of c is $\overline{u}_{\Omega}$, the average of u over the domain.

LEMMA 3.4 (Poincaré's inequality). *Consider a John domain $\Omega \in \mathbb{R}^2$. Then*

$$\|u - \overline{u}_{\Omega}\|^2_{L^2(\Omega)} \leq C|\Omega| \|\nabla u\|^2_{L^2(\Omega)}, \ \forall u \in H(\text{grad}, \Omega),$$

where the constant C depends on the John constant $C_J(\Omega)$.

We also need the following discrete Sobolev inequality, proved in [7, Lemma 3.2] for John domains:

ETNA
Kent State University
http://etna.math.kent.edu

LEMMA 3.5. *For $u \in W^h_{\mathrm{grad}}(\Omega)$, there exists a constant C such that*

$$\|u\|^2_{L^\infty(\Omega)} \leq C\left(1+\log\frac{H}{h}\right)\|u\|^2_{H^1(\Omega)}, \text{ and}$$

$$\|u-\overline{u}_\Omega\|^2_{L^\infty(\Omega)} \leq C\left(1+\log\frac{H}{h}\right)|u|^2_{H^1(\Omega)},$$

where

$$\|u\|^2_{H^1(\Omega)} := |u|^2_{H^1(\Omega)} + \frac{1}{H^2}\|u\|^2_{L^2(\Omega)}$$

and $\operatorname{diam}(\Omega) = H$. *The constant C depends on the John constant $C_J(\Omega)$, and the shape regularity of the elements.*

4. Technical tools. The auxiliary results presented in this section will be used in the proof of our main results, Theorems 5.1 and 5.2.

4.1. Cutoff functions. We introduce a new cutoff function that will be used later for the construction of local functions with support in $\Omega_i \cap \Omega'_j$.

LEMMA 4.1. *Let $\mathcal{E} \in S_{\mathcal{E}_i}$ with endpoints $\boldsymbol{a}$ and $\boldsymbol{b}$. Then there exists a function $\theta^\delta_{\mathcal{E}} \in W^{h_i}_{\mathrm{grad}}(\Omega_i)$ that takes the value 1 at the nodes on $\mathcal{E}$, vanishes in $\Omega_i \setminus \Omega'_j$, and such that*

$$\|\nabla\theta^\delta_{\mathcal{E}}\|^2_{L^2(\Omega_i\cap\Omega'_j)} \leq C\chi_{\mathcal{E}}(\delta_i)\left(1+\frac{d_{\mathcal{E}}}{\delta_i}\right)\left(1+\log\frac{\delta_i}{h_i}\right), \tag{4.1}$$

for some constant C depending on C_J and the shape regularity of the elements.

Proof. For the proof of this lemma, we use similar ideas as in [9, Lemma 2.7] and [10, Lemma 3.6]. Rename $\mathcal{E}_1 := \mathcal{E}$ and let $\mathcal{E}_2 := \partial\left(\Omega_i \cap \Omega'_j\right) \setminus \mathcal{E}$. Split $\mathcal{E}_2$ into two subsets, $\mathcal{E}_3 := \mathcal{E}_2 \cap \partial\Omega'_j$ and $\mathcal{E}_4 := \mathcal{E}_2 \setminus \mathcal{E}_3$. Note that $\mathcal{E}_4$ is a subset of $\partial\Omega_i$ with two components, one with $\boldsymbol{a}$ and the other with $\boldsymbol{b}$ as endpoints. Denote by $d_i(\boldsymbol{x})$ the distance of $\boldsymbol{x}$ to the edge $\mathcal{E}_i$ and consider the function $\tilde{\theta}_{\mathcal{E}}$ given by

$$\tilde{\theta}_{\mathcal{E}}(\boldsymbol{x}) := \frac{1/d_1(\boldsymbol{x})}{1/d_1(\boldsymbol{x}) + 1/d_2(\boldsymbol{x})}$$

for $\boldsymbol{x} \in \Omega_i \cap \Omega'_j$ and by zero everywhere else in Ω_i. At the endpoints $\boldsymbol{a}$ and $\boldsymbol{b}$, we set this function to zero. Note that this function vanishes on $\mathcal{E}_2$ and takes the required values on $\mathcal{E}$. We then define $\theta^\delta_{\mathcal{E}} := I^h(\tilde{\theta}_{\mathcal{E}})$.

We first note that the contribution from any element with $\boldsymbol{a}$ or $\boldsymbol{b}$ as a vertex is bounded, because the gradient of the interpolant is bounded by $1/h_i$, since all the nodal values are between 0 and 1.

We next estimate the energy over all the elements that do not intersect the endpoints and lie inside $\Omega_i \cap \Omega'_j$. We denote this region by $\mathcal{R}$. It is easy to prove that

$$|\nabla\tilde{\theta}_{\mathcal{E}}(\boldsymbol{x})| \leq \frac{1}{d_1(\boldsymbol{x}) + d_2(\boldsymbol{x})}.$$

We divide $\mathcal{R}$ into two disjoint sets, $\mathcal{R}_1 := \{\boldsymbol{x} \in \mathcal{R} : d_3(\boldsymbol{x}) \leq d_4(\boldsymbol{x})\}$, and $\mathcal{R}_2$, its complement.

First, for $\boldsymbol{x} \in \mathcal{R}_1$, we note that $d_2(\boldsymbol{x}) = d_3(\boldsymbol{x})$. Let $\boldsymbol{x}_1$ and $\boldsymbol{x}_3$ be the points on $\mathcal{E}_1$ and $\mathcal{E}_3$ closest to $\boldsymbol{x}$. We have $\delta_i \leq d(\boldsymbol{x}_1, \mathcal{E}_3) \leq |x_1 - x_3| \leq d_1(\boldsymbol{x}) + d_3(\boldsymbol{x})$ and then $|\nabla\tilde{\theta}_{\mathcal{E}}(\boldsymbol{x})| \leq 1/\delta_i$.

ETNA
Kent State University
http://etna.math.kent.edu

As in [7, Section 4], we cover the set with square patches with diameters of the order of δ_i and note that on the order of $\chi_{\mathcal{E}}(\delta_i)d_{\mathcal{E}}/\delta_i$ of them will suffice. The contribution of each square is bounded, and therefore

$$\int_{\mathcal{R}_1} |\nabla \tilde{\theta}_{\mathcal{E}}(\boldsymbol{x})|^2 d\boldsymbol{x} \leq C\chi_{\mathcal{E}}(\delta_i)\frac{d_{\mathcal{E}}}{\delta_i}.$$

Second, for $\boldsymbol{x} \in \mathcal{R}_2$, we note that $d_2(\boldsymbol{x}) = d_4(\boldsymbol{x})$. We claim that $d_1(\boldsymbol{x})+d_4(\boldsymbol{x}) \geq Cr(\boldsymbol{x})$, where $r(\boldsymbol{x})$ is the minimal distance of $\boldsymbol{x}$ to $\boldsymbol{a}$ and $\boldsymbol{b}$. This implies that

$$\int_{\mathcal{R}_2} |\nabla \tilde{\theta}_{\mathcal{E}}(\boldsymbol{x})|^2 d\boldsymbol{x} \leq C\int_{\mathcal{R}_2} \frac{1}{r^2(\boldsymbol{x})} d\boldsymbol{x} \leq C\log\frac{\delta_i}{h_i},$$

by using polar coordinates centered at $\boldsymbol{a}$ and $\boldsymbol{b}$. From the last two inequalities, and the fact that $|\nabla\theta^{\delta}_{\mathcal{E}}| = |\nabla I^h(\tilde{\theta}_{\mathcal{E}})| \leq C\max_{x\in K}|\nabla\tilde{\theta}_{\mathcal{E}}|$, we obtain (4.1).

All that is left is to show that $d_1(\boldsymbol{x}) + d_4(\boldsymbol{x}) \geq Cr(\boldsymbol{x})$ for some constant C. Without loss of generality, assume that $|\boldsymbol{x}-\boldsymbol{a}| \leq |\boldsymbol{x}-\boldsymbol{b}|$. Consider the curve $\gamma(t)$ in the Definition 3.1 between $\boldsymbol{x}_0$ and $\boldsymbol{a}$, and let $\boldsymbol{x}_\gamma$ be the point on γ which is closest to $\boldsymbol{x}$. By the triangle inequality and the definition of a John domain, we have that

$$r(\boldsymbol{x}) = |\boldsymbol{x}-\boldsymbol{a}| \leq |\boldsymbol{x}-\boldsymbol{x}_\gamma| + C_J dist(\boldsymbol{x}_\gamma, \mathcal{E}_1).$$

Again by the triangle inequality and the fact that $dist(\boldsymbol{x}_\gamma, \mathcal{E}_1) \leq |\boldsymbol{x}_\gamma - \boldsymbol{x}_1|$, where $\boldsymbol{x}_1$ is the point on $\mathcal{E}_1$ closest to $\boldsymbol{x}$, we obtain

$$r(\boldsymbol{x}) \leq (C_J+1)\,|\boldsymbol{x}-\boldsymbol{x}_\gamma| + C_J|\boldsymbol{x}-\boldsymbol{x}_1|.$$

We notice that if $\boldsymbol{x}$ lies in the region between γ and $\mathcal{E}$, then $|\boldsymbol{x}-\boldsymbol{x}_\gamma| \leq d_4(\boldsymbol{x})$ and if not, then $|\boldsymbol{x}-\boldsymbol{x}_\gamma| \leq d_1(\boldsymbol{x})$. In both cases we can deduce that $|\boldsymbol{x}-\boldsymbol{x}_\gamma| \leq d_1(\boldsymbol{x}) + d_4(\boldsymbol{x})$. This concludes the proof of the lemma. ∎

From the proof of Lemma 4.1, we can estimate the diameter and area of $\Omega_i \cap \Omega'_j$:

LEMMA 4.2. *For each coarse edge $\mathcal{E}^{ij} \in S_{\mathcal{E}_i}$, we have that*

$$\begin{aligned}\text{diam}\,(\Omega_i \cap \Omega'_j) &\leq C\chi_{\mathcal{E}}(\delta_i)d_{\mathcal{E}}, \text{and}\\ |\Omega_i \cap \Omega'_j| &\leq C\chi_{\mathcal{E}}(\delta_i)d_{\mathcal{E}}\delta_i.\end{aligned}$$

Proof. Consider the covering by squares in the proof of Lemma 4.1. Given two points $x, y \in \Omega_i \cap \Omega'_j$, we can join them by segments that lie in the interior of a certain number of squares. Each of these segments have a length less than $\sqrt{2}\delta_i$ and since the total number of squares is on the order of $\chi_{\mathcal{E}}(\delta_i)d_{\mathcal{E}}/\delta_i$, we can conclude that the diameter of $\Omega_i \cap \Omega'_j$ is bounded by $C\chi_{\mathcal{E}}(\delta_i)d_{\mathcal{E}}$. The second inequality follows by adding the area of all the squares that cover $\Omega_i \cap \Omega'_j$. ∎

4.2. An inverse inequality. We present an inverse inequality for elements in the space $W^{h_i}_{\text{curl}}(\Omega_i)$ which will be used in our discussion. First, we have the following elementary estimates for a function in $W^{h_i}_{\text{curl}}(\Omega_i)$ in terms of its degrees of freedom defined in (2.1).

LEMMA 4.3. *Let $K \in \mathcal{T}_{h_i}$. Then, there exist positive constants c and C, depending only on the aspect ratio of K, such that for all $\boldsymbol{u} \in W^{h_i}_{\text{curl}}(\Omega_i)$,*

$$c\sum_{e\in\partial K} h_e^2\lambda_e(\boldsymbol{u})^2 \leq \|\boldsymbol{u}\|^2_{L^2(K)} \leq C\sum_{e\in\partial K} h_e^2\lambda_e(\boldsymbol{u})^2, \text{ and}$$

ETNA
Kent State University
http://etna.math.kent.edu

$$\|\nabla \times \boldsymbol{u}\|^2_{L^2(K)} \leq C \sum_{e \in \partial K} \lambda_e(\boldsymbol{u})^2.$$

Proof. See [24, Proposition 6.3.1] and [32, Lemma 3.1]. ∎

Combining these two inequalities, we find an inverse inequality:

COROLLARY 4.4 (Inverse inequality). *For $\boldsymbol{u} \in W^{h_i}_{\mathrm{curl}}(\Omega_i)$, there exists a constant C that depends only on the aspect ratio of K, such that*

$$\|\nabla \times \boldsymbol{u}\|^2_{L^2(K)} \leq C h_i^{-2} \|\boldsymbol{u}\|^2_{L^2(K)}.$$

4.3. Estimates for auxiliary functions. We start by introducing a linear interpolant for functions in $W^{h_i}_{\mathrm{grad}}(\Omega_i)$. Consider an edge $\mathcal{E} \in S_{\mathcal{E}_i}$ with endpoints $\boldsymbol{a}$ and $\boldsymbol{b}$, and moving from $\boldsymbol{a}$ past $\boldsymbol{b}$, pick a point $\boldsymbol{c}$ on $\partial\Omega_i$, such that $|\boldsymbol{c} - \boldsymbol{b}|$ is of order $d_{\mathcal{E}}$. Consider the function $\theta_{\boldsymbol{b}\ell} \in W^{h_i}_{\mathrm{grad}}(\Omega_i)$ constructed in [9, Lemma 2.7] for the points $\boldsymbol{a}, \boldsymbol{b}$ and $\boldsymbol{c}$. This function is uniformly bounded in Ω_i, $\theta_{\boldsymbol{b}\ell}(\boldsymbol{a}) = 0$, $\theta_{\boldsymbol{b}\ell}(\boldsymbol{b}) = 1$, and also satisfies

$$\|\nabla \theta_{\boldsymbol{b}\ell}\|^2_{L^2(\Omega_i)} \leq C, \text{and } \nabla \theta_{\boldsymbol{b}\ell} \cdot \boldsymbol{t}_e = \frac{1}{d_{\mathcal{E}}} \boldsymbol{d}_{\mathcal{E}} \cdot \boldsymbol{t}_e$$

along $\mathcal{E}$. Using this function, we introduce our linear interpolant:

DEFINITION 4.5 (linear interpolant). *Given $f \in W^{h_i}_{\mathrm{grad}}(\Omega_i)$ and a subdomain edge $\mathcal{E} \in S_{\mathcal{E}_i}$ with endpoints $\boldsymbol{a}$ and $\boldsymbol{b}$, we define the linear function*

$$f^{\mathcal{E}\ell}(\boldsymbol{x}) := f(\boldsymbol{a}) + (f(\boldsymbol{b}) - f(\boldsymbol{a}))\, \theta_{\boldsymbol{b}\ell}(\boldsymbol{x}).$$

We note that $f^{\mathcal{E}\ell}(\boldsymbol{a}) = f(\boldsymbol{a})$, $f^{\mathcal{E}\ell}(\boldsymbol{b}) = f(\boldsymbol{b})$, and

$$\nabla f^{\mathcal{E}\ell}(\boldsymbol{x}) \cdot \boldsymbol{t}_e = \frac{f(\boldsymbol{b}) - f(\boldsymbol{a})}{d_{\mathcal{E}}} \boldsymbol{d}_{\mathcal{E}} \cdot \boldsymbol{t}_e$$

along $\mathcal{E}$. We will need the following auxiliary results:

LEMMA 4.6. *Let u be a continuous piecewise quadratic function defined on $\mathcal{T}_h$ and let $I^h u$ be its piecewise linear interpolant on the same mesh, defined by (2.2). Then, there exists a constant C, independent of h, such that*

$$|I^h u|_{H^1(K)} \leq C |u|_{H^1(K)} \text{ for } K \in \mathcal{T}_h.$$

Proof. See [31, Lemma 3.9]. ∎

LEMMA 4.7. *For any $p \in W^{h_i}_{\mathrm{grad}}(\Omega_i)$, there exists a function $p^{\mathcal{E}\Delta} \in W^{h_i}_{\mathrm{grad}}(\Omega_i)$ such that $p^{\mathcal{E}\Delta} = p - p^{\mathcal{E}\ell}$ along $\mathcal{E}$. This function vanishes along $\partial\left(\Omega_i \cap \Omega_j'\right) \setminus \mathcal{E}$ and $\partial\Omega_i \setminus \mathcal{E}$, and satisfies*

$$\|\nabla p^{\mathcal{E}\Delta}\|^2_{L^2(\Omega_i)} \leq C \chi_{\mathcal{E}}(\delta_i) \left(1 + \log \frac{\delta_i}{h_i}\right) \left(1 + \frac{d_{\mathcal{E}}}{\delta_i}\right) \left(1 + \log \frac{H_i}{h_i}\right) \|\nabla p\|^2_{L^2(\Omega_i)}$$

for some constant C depending on C_J and the shape regularity of the elements.

Proof. We define $p^{\mathcal{E}\Delta} := I^{h_i}(\theta^{\delta}_{\mathcal{E}}(p - p^{\mathcal{E}\ell}))$. We use the inequality

$$|p(\boldsymbol{b}) - p(\boldsymbol{a})|^2 \leq C \left(1 + \log \frac{H_i}{h_i}\right) \|\nabla p\|^2_{L^2(\Omega_i)},$$

ETNA
Kent State University
http://etna.math.kent.edu

which follows from Lemma 3.5, and since $p - p^{\mathcal{E}\ell} = (p - p(\boldsymbol{a})) - (p^{\mathcal{E}\ell} - p(\boldsymbol{a}))$, we have

$$\|p - p^{\mathcal{E}\ell}\|^2_{L^\infty(\Omega_i \cap \Omega_j')} \leq C \left(1 + \log \frac{H_i}{h_i}\right) \|\nabla p\|^2_{L^2(\Omega_i)}.$$

Since $\nabla p^{\mathcal{E}\ell}(\boldsymbol{x}) = (p(\boldsymbol{b}) - p(\boldsymbol{a}))\, \nabla \theta_{\boldsymbol{b}\ell}(\boldsymbol{x})$, we have

$$\|\nabla p^{\mathcal{E}\ell}\|^2_{L^2(\Omega_i \cap \Omega_j')} \leq C \left(1 + \log \frac{H_i}{h_i}\right) \|\nabla p\|^2_{L^2(\Omega_i)}.$$

From these estimates, Lemma 4.1 and

$$\nabla(\theta^\delta_{\mathcal{E}}(p - p^{\mathcal{E}\ell})) = \nabla \theta^\delta_{\mathcal{E}}(p - p^{\mathcal{E}\ell}) + \nabla(p - p^{\mathcal{E}\ell})\theta^\delta_{\mathcal{E}},$$

we find that

$$|\theta^\delta_{\mathcal{E}}(p - p^{\mathcal{E}\ell})|^2_{H(\mathrm{grad},\Omega_i)} \leq C\chi_{\mathcal{E}}(\delta_i) \left(1 + \log \frac{\delta_i}{h_i}\right) \left(1 + \frac{d_{\mathcal{E}}}{\delta_i}\right) \left(1 + \log \frac{H_i}{h_i}\right) \|\nabla p\|^2_{L^2(\Omega_i)}.$$

The result then follows by using Lemma 4.6. ∎

LEMMA 4.8. *Given $\boldsymbol{r} \in W^{h_i}_{\mathrm{curl}}(\Omega_i)$ and a subdomain edge $\mathcal{E} \in S_{\mathcal{E}_i}$, it holds that*

$$|\overline{r}_{\mathcal{E}}|^2 \leq C \left(\|\boldsymbol{r}\|^2_{L^\infty(\Omega_i)} + \|\nabla \times \boldsymbol{r}\|^2_{L^2(\Omega_i)}\right),$$

where

$$\overline{r}_{\mathcal{E}} := \frac{1}{d_{\mathcal{E}}} \int_{\mathcal{E}} \boldsymbol{r} \cdot \boldsymbol{t}_{\mathcal{E}} ds \tag{4.2}$$

and the constant C depends only on the John parameter $C_J(\Omega_i)$.

Proof. A similar bound is obtained in the proof of [10, Lemma 3.10] over a subset of Ω_i, from which our result follows. ∎

LEMMA 4.9. *Given $\mathcal{E} \in S_{\mathcal{E}_i}$, there exists a coarse space function $\boldsymbol{N}_{\mathcal{E}} \in W^{h_i}_{\mathrm{curl}}(\Omega_i)$ that vanishes in $\Omega_i \setminus \Omega_j'$, with $\boldsymbol{N}_{\mathcal{E}} \cdot \boldsymbol{t}_e = \boldsymbol{d}_{\mathcal{E}} \cdot \boldsymbol{t}_e$ along $\mathcal{E}$, and $\boldsymbol{N}_{\mathcal{E}} \cdot \boldsymbol{t}_e = 0$ everywhere else on $\partial\Omega_i$, such that*

$$\|\boldsymbol{N}_{\mathcal{E}}\|^2_{L^2(\Omega_i)} \leq C\chi_{\mathcal{E}}(\delta_i) d_{\mathcal{E}} \delta_i,$$

$$\|\nabla \times \boldsymbol{N}_{\mathcal{E}}\|^2_{L^2(\Omega_i)} \leq C\chi_{\mathcal{E}}(\delta_i) \left(1 + \log \frac{\delta_i}{h_i}\right) \left(1 + \frac{d_{\mathcal{E}}}{\delta_i}\right),$$

for some constant C depending on C_J and the shape regularity of the elements.

Proof. Consider the function

$$\boldsymbol{N}_{\mathcal{E}} := \Pi^{h_i}(\theta^\delta_{\mathcal{E}} \boldsymbol{d}_{\mathcal{E}}) + \boldsymbol{b}_{\mathcal{E}}/2,$$

where

$$\boldsymbol{b}_{\mathcal{E}} := (\boldsymbol{d}_{\mathcal{E}} \cdot \boldsymbol{t}_{e_a}) \boldsymbol{N}_{e_a} + (\boldsymbol{d}_{\mathcal{E}} \cdot \boldsymbol{t}_{e_b}) \boldsymbol{N}_{e_b},$$

and e_a, e_b are the two finite element edges at the ends of $\mathcal{E}$. It is easy to check that $\boldsymbol{N}_{\mathcal{E}}$ has the specified tangential data and that it vanishes in $\Omega_i \setminus \Omega_j'$.

ETNA
Kent State University
http://etna.math.kent.edu

Following [10, Lemma 3.11]. we can prove that

$$\|\boldsymbol{b}_{\mathcal{E}}\|^2_{L^2(\Omega_i)} \leq Ch_i^2, \|\nabla \times \boldsymbol{b}_{\mathcal{E}}\|^2_{L^2(\Omega_i)} \leq C,$$

$$\|\Pi^{h_i}(\theta^{\delta}_{\mathcal{E}}\boldsymbol{d}_{\mathcal{E}})\|^2_{L^2(\Omega_i)} \leq C\chi_{\mathcal{E}}(\delta_i)d_{\mathcal{E}}\delta_i, \text{ and}$$

$$\|\nabla \times \Pi^{h_i}(\theta^{\delta}_{\mathcal{E}}\boldsymbol{d}_{\mathcal{E}})\|^2_{L^2(\Omega_i)} \leq C\chi_{\mathcal{E}}(\delta_i)\left(1+\log\frac{\delta_i}{h_i}\right)\left(1+\frac{d_{\mathcal{E}}}{\delta_i}\right),$$

where we have used Lemmas 4.1 and 4.2. The lemma follows by combining these inequalities. ∎

LEMMA 4.10. *Given $\boldsymbol{r} \in W^{h_i}_{\text{curl}}(\Omega_i)$ and an edge $\mathcal{E} \in S_{\mathcal{E}_i}$, there exists a function $\boldsymbol{r}^{\mathcal{E}} \in W^{h_i}_{\text{curl}}(\Omega_i)$ that vanishes in $\Omega_i \setminus \Omega'_j$, such that $\boldsymbol{r}^{\mathcal{E}} \cdot \boldsymbol{t}_e = \boldsymbol{r} \cdot \boldsymbol{t}_e$ along $\mathcal{E}$, and with vanishing tangential data along $\partial(\Omega_i \cap \Omega'_j) \setminus \mathcal{E}$ and $\partial\Omega_i \setminus \mathcal{E}$. Further,*

$$\|\boldsymbol{r}^{\mathcal{E}}\|^2_{L^2(\Omega_i)} \leq C\chi_{\mathcal{E}}(\delta_i)d_{\mathcal{E}}\delta_i\|\boldsymbol{r}\|^2_{L^\infty(\Omega_i\cap\Omega'_j)}, \text{ and}$$

$$\|\nabla \times \boldsymbol{r}^{\mathcal{E}}\|^2_{L^2(\Omega_i)} \leq C\Big(\|\nabla \times \boldsymbol{r}\|^2_{L^2(\Omega_i\cap\Omega'_j)} + \\ + \chi_{\mathcal{E}}(\delta_i)\left(1+\log\frac{\delta_i}{h_i}\right)\left(1+\frac{d_{\mathcal{E}}}{\delta_i}\right)\|\boldsymbol{r}\|^2_{L^\infty(\Omega_i\cap\Omega'_j)}\Big),$$

for some constant C depending on C_J and the shape regularity of the elements.

Proof. We write the function $\boldsymbol{r}$ in the Nédélec basis as

$$\boldsymbol{r} = \sum_{e\in M^{h_i}} r_e\boldsymbol{N}_e,$$

and define

$$\boldsymbol{r}^{\mathcal{E}} := \sum_{e\in M^{h_i}} \theta^{\delta,e}_{\mathcal{E}} r_e\boldsymbol{N}_e + \left(r_{e_a}\boldsymbol{N}_{e_a} + r_{e_b}\boldsymbol{N}_{e_b}\right)/2,$$

where $\theta^{\delta,e}_{\mathcal{E}}$ is the value of $\theta^{\delta}_{\mathcal{E}}$ at the middle point of e, and e_a, e_b are the edges at the ends of $\mathcal{E}$. As in [10, Lemma 3.12], we have that

$$\|r_{e_a}\boldsymbol{N}_{e_a} + r_{e_b}\boldsymbol{N}_{e_b}\|^2_{L^2(\Omega_i)} \leq Ch_i^2\|\boldsymbol{r}\|^2_{L^\infty(\Omega_i\cap\Omega'_j)},$$
$$\|\nabla \times \left(r_{e_a}\boldsymbol{N}_{e_a} + r_{e_b}\boldsymbol{N}_{e_b}\right)\|^2_{L^2(\Omega_i)} \leq C\|\boldsymbol{r}\|^2_{L^\infty(\Omega_i\cap\Omega'_j)},$$
$$\left\|\sum_{e\in M^{h_i}} \theta^{\delta,e}_{\mathcal{E}} r_e\boldsymbol{N}_e\right\|^2_{L^2(\Omega_i)} \leq C\|\boldsymbol{r}\|^2_{L^2(\Omega_i\cap\Omega'_j)}, \text{ and}$$

$$\left\|\sum_{e\in M^{h_i}} \nabla \times \theta^{\delta,e}_{\mathcal{E}} r_e\boldsymbol{N}_e\right\|^2_{L^2(\Omega_i)} \leq C\Big(\|\nabla \times \boldsymbol{r}\|_{L^2(\Omega_i\cap\Omega'_j)} + \\ + \|\boldsymbol{r}\|^2_{L^\infty(\Omega_i\cap\Omega'_j)}\|\nabla\theta^{\delta}_{\mathcal{E}}\|^2_{L^2(\Omega_i\cap\Omega'_j)}\Big).$$

We conclude our proof by using Lemmas 4.1 and 4.2. ∎

ETNA
Kent State University
http://etna.math.kent.edu

4.4. A Helmholtz decomposition. The following lemma is [10, Lemma 3.14]:

LEMMA 4.11. *Given a John domain D of diameter d and $\boldsymbol{u} \in W^{h_i}_{\mathrm{curl}}(D)$, there exist $p \in W^{h_i}_{\mathrm{grad}}(D)$, $\boldsymbol{r} \in W^{h_i}_{\mathrm{curl}}(D)$ and a constant C such that*

$$\boldsymbol{u} = \nabla p + \boldsymbol{r},$$

$$\|\nabla p\|^2_{L^2(D)} \leq C \left(\|\boldsymbol{u}\|^2_{L^2(D)} + d^2 \|\nabla \times \boldsymbol{u}\|^2_{L^2(D)} \right), \text{ and} \tag{4.3a}$$

$$\|\boldsymbol{r}\|^2_{L^\infty(D)} \leq C \left(1 + \log\left(d/h_i\right)\right) \|\nabla \times \boldsymbol{u}\|^2_{L^2(D)}. \tag{4.3b}$$

The constant C depends on D and the shape regularity of the mesh.

5. The algorithm and the main result. Our algorithm is an additive two-level Schwarz method; see [31, Chapters 2 and 3]. We obtain the overlapping regions Ω_i' by adding a number of layers of elements to Ω_i and use exact local solvers over the Ω_i'. We consider the coarse space

$$V_0 := \left\{ \boldsymbol{w} \in W^h_{\mathrm{curl}}(\Omega) : \boldsymbol{w} = \sum_{\mathcal{E} \in S_\mathcal{E}} \alpha_\mathcal{E} \boldsymbol{c}_\mathcal{E} \right\},$$

where the coarse functions $\boldsymbol{c}_\mathcal{E}$ were introduced at the end of Section 2, and the local spaces

$$V_i := \left\{ \boldsymbol{w}_i \in W^{h_i}_{\mathrm{curl}}(\Omega_i') : \boldsymbol{w}_i = \sum_{e \in M_i} \alpha_e \boldsymbol{N}_e \right\},$$

where M_i is the set of element edges in Ω_i', $1 \leq i \leq N$. The space $W^h_{\mathrm{curl}}(\Omega)$ can be written as $R_0^T V_0 + \sum R_i^T V_i$, where $R_i^T : V_i \to V$ are the natural extension operators.

We define the coarse matrix by $A_0 := R_0 A R_0^T$ and the local matrices by $A_i := R_i A R_i^T$, where A is the stiffness matrix associated to problem (1.2). The Schwarz operators are defined as $P_i := R_i^T A_i^{-1} R_i A$, $0 \leq i \leq N$.

By [31, Theorem 2.7], the condition number of the additive operator

$$P_{ad} := \sum_{i=0}^{N} P_i$$

is bounded by

$$\kappa(P_{ad}) \leq (N^C + 1) C_0^2, \tag{5.1}$$

where N^C is the minimum number of colors needed to color the subdomains associated with the local subproblems such that no pair of subdomains of the same color intersect; see [31, Section 3.6]. The constant C_0^2 is a bound for the energy of a splitting

$$\boldsymbol{u} = R_0^T \boldsymbol{u}_0 + \sum_{i=1}^{N} R_i^T \boldsymbol{u}_i$$

for $\boldsymbol{u} \in W^h_{\mathrm{curl}}(\Omega)$ given by

$$a(\boldsymbol{u}_0, \boldsymbol{u}_0) + \sum_{i=1}^{N} a_i'(\boldsymbol{u}_i, \boldsymbol{u}_i) \leq C_0^2 a(\boldsymbol{u}, \boldsymbol{u}).$$

We can also consider multiplicative and hybrid Schwarz algorithms; see [31, Section 2.2] and Example 6.7.

ETNA
Kent State University
http://etna.math.kent.edu

5.1. The coarse space component. In this section, we build an explicit function that will provide a bound for the coarse function $\boldsymbol{u}_0$ defined in (2.3). We consider the Helmholtz decomposition of Lemma 4.11 for each John domain Ω_i and write $\boldsymbol{u} = \nabla p_i + \boldsymbol{r}_i$. We have

$$\overline{u}_{\mathcal{E}} = \frac{p_i(\boldsymbol{b}) - p_i(\boldsymbol{a})}{d_{\mathcal{E}}} + \frac{1}{d_{\mathcal{E}}} \int_{\mathcal{E}} \boldsymbol{r}_i \cdot \boldsymbol{t}_{\mathcal{E}} ds. \tag{5.2}$$

For any edge $\mathcal{E} \in S_{\mathcal{E}_i}$, we define the function

$$\boldsymbol{w}_i^{\mathcal{E}} := \nabla p_i^{\mathcal{E}\Delta} + \boldsymbol{r}_i^{\mathcal{E}} - \overline{r}_{i\mathcal{E}} \boldsymbol{N}_{\mathcal{E}}, \tag{5.3}$$

where $\nabla p_i^{\mathcal{E}\Delta}$, $\boldsymbol{N}_{\mathcal{E}}$ and $\boldsymbol{r}_i^{\mathcal{E}}$ are the functions from Lemmas 4.7, 4.9 and 4.10 respectively, and $\overline{r}_{i\mathcal{E}}$ is given by (4.2). By construction, $\boldsymbol{w}_i^{\mathcal{E}}$ vanishes in $\Omega_i \setminus \Omega_j'$. We define $\boldsymbol{w}_j^{\mathcal{E}}$ over $\Omega_j \cap \Omega_i'$, similarly. We first find that

$$\begin{aligned} \boldsymbol{w}_i^{\mathcal{E}} \cdot \boldsymbol{t}_e &= \nabla p_i \cdot \boldsymbol{t}_e + \boldsymbol{r}_i \cdot \boldsymbol{t}_e - \nabla p_i^{\mathcal{E}\ell} \cdot \boldsymbol{t}_e - \overline{r}_{i\mathcal{E}} \boldsymbol{N}_{\mathcal{E}} \cdot \boldsymbol{t}_e \\ &= (\boldsymbol{u} - \boldsymbol{u}_0) \cdot \boldsymbol{t}_e \end{aligned}$$

along $\mathcal{E}$, where we have used (5.2) in the last step. Similarly $\boldsymbol{w}_j^{\mathcal{E}} \cdot \boldsymbol{t}_e = (\boldsymbol{u} - \boldsymbol{u}_0) \cdot \boldsymbol{t}_e$. Hence, the function $\boldsymbol{w}^{\mathcal{E}}$ given by

$$\boldsymbol{w}^{\mathcal{E}}(\boldsymbol{x}) := \begin{cases} \boldsymbol{w}_i^{\mathcal{E}}(\boldsymbol{x}) & \text{if } \boldsymbol{x} \in \Omega_i \cap \Omega_j' \\ \boldsymbol{w}_j^{\mathcal{E}}(\boldsymbol{x}) & \text{if } \boldsymbol{x} \in \Omega_j \cap \Omega_i' \end{cases}$$

is well-defined and belongs to $W^{h_i}_{\mathrm{curl}}(\Omega)$, since its tangential data is continuous across $\mathcal{E}$ (in fact, it is equal to the tangential component of $\boldsymbol{u} - \boldsymbol{u}_0$). We note that $\boldsymbol{w}^{\mathcal{E}}$ is supported in $\Omega_i' \cap \Omega_j'$ and vanishes in $(\Omega_i \setminus \Omega_j') \cup (\Omega_j \setminus \Omega_i')$.

Finally, consider the function

$$\boldsymbol{g} := \boldsymbol{u} - \sum_{\mathcal{E} \in S_{\mathcal{E}}} \boldsymbol{w}^{\mathcal{E}}. \tag{5.4}$$

We find that $\boldsymbol{g} \cdot \boldsymbol{t}_e = \boldsymbol{u}_0 \cdot \boldsymbol{t}_e$ along the interface. Thus $\boldsymbol{g}$ has the same tangential data as $\boldsymbol{u}_0$ along the interface, and therefore its energy will provide an upper bound for the energy of $\boldsymbol{u}_0$, since $\boldsymbol{u}_0$ minimizes the energy for the specified boundary data.

We next find bounds for the energy of the components of $\boldsymbol{w}^{\mathcal{E}}$. First, from Lemma 4.7 and (4.3a), we easily deduce that

$$\begin{aligned} a_i(\nabla p_i^{\mathcal{E}\Delta}, \nabla p_i^{\mathcal{E}\Delta}) &= \beta_i \|\nabla p_i^{\mathcal{E}\Delta}\|^2_{L^2(\Omega_i)} \\ &\leq C \chi_{\mathcal{E}}(\delta_i) \eta_i \left(1 + \log \frac{\delta_i}{h_i}\right) \left(1 + \frac{H_i}{\delta_i}\right) \left(1 + \log \frac{H_i}{h_i}\right) a_i(\boldsymbol{u}, \boldsymbol{u}), \end{aligned} \tag{5.5}$$

where $\eta_i := 1 + \beta_i H_i^2 / \alpha_i$.

For the second term of (5.3), we get from Lemma 4.10 and (4.3b),

$$\alpha_i \|\nabla \times \boldsymbol{r}_i^{\mathcal{E}}\|^2_{L^2(\Omega_i)} \leq C \chi_{\mathcal{E}}(\delta_i) \left(1 + \log \frac{\delta_i}{h_i}\right) \left(1 + \frac{H_i}{\delta_i}\right) \left(1 + \log \frac{H_i}{h_i}\right) a_i(\boldsymbol{u}, \boldsymbol{u}), \tag{5.6}$$

where we have replaced $\nabla \times \boldsymbol{r}_i$ by $\nabla \times \boldsymbol{u}$, since $\nabla \times \nabla p_i = 0$. Also,

$$\begin{aligned} \beta_i \|\boldsymbol{r}_i^{\mathcal{E}}\|^2_{L^2(\Omega_i)} &\leq C \chi_{\mathcal{E}}(\delta_i) \beta_i d_{\mathcal{E}} \delta_i \left(1 + \log \frac{H_i}{h_i}\right) \|\nabla \times \boldsymbol{u}\|^2_{L^2(\Omega_i)} \\ &\leq C \chi_{\mathcal{E}}(\delta_i) \frac{\beta_i H_i^2}{\alpha_i} \left(1 + \log \frac{H_i}{h_i}\right) a_i(\boldsymbol{u}, \boldsymbol{u}). \end{aligned} \tag{5.7}$$

ETNA
Kent State University
http://etna.math.kent.edu

From (5.6) and (5.7), we get

$$a_i(\boldsymbol{r}_i^{\mathcal{E}}, \boldsymbol{r}_i^{\mathcal{E}}) \leq C\chi_{\mathcal{E}}(\delta_i)\eta_i \left(1+\log\frac{\delta_i}{h_i}\right)\left(1+\frac{H_i}{\delta_i}\right)\left(1+\log\frac{H_i}{h_i}\right) a_i(\boldsymbol{u},\boldsymbol{u}). \tag{5.8}$$

Next, from Lemmas 4.8 and (4.3b),

$$\begin{aligned}|\overline{r}_{i\mathcal{E}}|^2 &\leq C\left(\|\boldsymbol{r}_i\|^2_{L^\infty(\Omega_i)} + \|\nabla\times\boldsymbol{r}_i\|^2_{L^2(\Omega_i)}\right)\\ &\leq C\left(1+\log\frac{H_i}{h_i}\right)\|\nabla\times\boldsymbol{u}\|^2_{L^2(\Omega_i)}.\end{aligned}$$

Hence, by Lemma 4.9,

$$\begin{aligned}a_i(\overline{r}_{i\mathcal{E}}\boldsymbol{N}_{\mathcal{E}}, \overline{r}_{i\mathcal{E}}\boldsymbol{N}_{\mathcal{E}}) &= |\overline{r}_{i\mathcal{E}}|^2\left(\alpha_i\|\nabla\times\boldsymbol{N}_{\mathcal{E}}\|^2_{L^2(\Omega_i)} + \beta_i\|\boldsymbol{N}_{\mathcal{E}}\|^2_{L^2(\Omega_i)}\right)\\ &\leq C\chi_{\mathcal{E}}(\delta_i)\eta_i\left(1+\log\frac{\delta_i}{h_i}\right)\left(1+\frac{H_i}{\delta_i}\right)\left(1+\log\frac{H_i}{h_i}\right) a_i(\boldsymbol{u},\boldsymbol{u}),\end{aligned} \tag{5.9}$$

by a similar argument as in (5.7). From (5.5), (5.8) and (5.9), we conclude that

$$a_i(\boldsymbol{w}_i^{\mathcal{E}}, \boldsymbol{w}_i^{\mathcal{E}}) \leq C\chi_{\mathcal{E}}(\delta_i)\eta_i \left(1+\log\frac{\delta_i}{h_i}\right)\left(1+\frac{H_i}{\delta_i}\right)\left(1+\log\frac{H_i}{h_i}\right) a_i(\boldsymbol{u},\boldsymbol{u}). \tag{5.10}$$

From (5.4) and (5.10), we conclude that

$$a(\boldsymbol{u}_0,\boldsymbol{u}_0) \leq a(\boldsymbol{g},\boldsymbol{g}) \leq C|\Xi|\chi\eta\left(1+\log\frac{\delta}{h}\right)\left(1+\frac{H}{\delta}\right)\left(1+\log\frac{H}{h}\right) a(\boldsymbol{u},\boldsymbol{u}), \tag{5.11}$$

where $\chi = \max\limits_i \max\limits_{\mathcal{E}\in S_{\mathcal{E}_i}} \chi_{\mathcal{E}}(\delta_i)$, $|\Xi|$ is the maximum number of subdomain edges for any subdomain, and $\eta := \max\limits_i \eta_i$. We note that $\eta_i \leq 2$ for the curl-dominated case, where $\beta_i H_i^2 \leq \alpha_i$. For the mass-dominated case, where $\beta_i H_i^2 > \alpha_i$, we cannot always remove the factor η, but see Theorem 5.2, Remarks 5.3 and 5.4 for some comments and bounds independent on η.

5.2. Local subspaces. For the decomposition in local components, we write

$$\boldsymbol{u}-\boldsymbol{u}_0 = (\boldsymbol{u}-\boldsymbol{g}) + (\boldsymbol{g}-\boldsymbol{u}_0) = \sum_{\mathcal{E}\in S_{\mathcal{E}}} \boldsymbol{w}^{\mathcal{E}} + \boldsymbol{w}_r,$$

with $\boldsymbol{w}_r := \boldsymbol{g}-\boldsymbol{u}_0$. We have that $\boldsymbol{w}_r\cdot\boldsymbol{t}_e = 0$ along the interface. Thus, we can write $\boldsymbol{w}_r = \sum_{i=1}^N \boldsymbol{w}_{ir}$, with $\boldsymbol{w}_{ir}$ the restriction of $\boldsymbol{w}_r$ to Ω_i. We can naturally consider a zero extension for $\boldsymbol{w}_{ir}$ to Ω_i', denoted still by $\boldsymbol{w}_{ir}$, that satisfies

$$a_i'(\boldsymbol{w}_{ir}, \boldsymbol{w}_{ir}) \leq C|\Xi|\chi\eta\left(1+\log\frac{\delta}{h}\right)\left(1+\frac{H}{\delta}\right)\left(1+\log\frac{H}{h}\right) a_i(\boldsymbol{u},\boldsymbol{u}). \tag{5.12}$$

We write also

$$\sum_{\mathcal{E}\in S_{\mathcal{E}}} \boldsymbol{w}^{\mathcal{E}} = \sum_{i=1}^N \boldsymbol{w}_{i\mathcal{E}},$$

ETNA
Kent State University
http://etna.math.kent.edu

with

$$\boldsymbol{w}_{i\mathcal{E}} := \frac{1}{2} \sum_{\mathcal{E} \in S_{\mathcal{E}_i}} \boldsymbol{w}^{\mathcal{E}}.$$

Note that $\boldsymbol{w}_{i\mathcal{E}}$ is supported in Ω_i' and satisfies

(5.13)
$$a_i'(\boldsymbol{w}_{i\mathcal{E}}, \boldsymbol{w}_{i\mathcal{E}}) \leq C|\Xi|\chi\eta \left(1 + \log \frac{\delta}{h}\right) \left(1 + \frac{H}{\delta}\right) \left(1 + \log \frac{H}{h}\right) (a_i(\boldsymbol{u}, \boldsymbol{u}) + a_j(\boldsymbol{u}, \boldsymbol{u})).$$

Therefore, we have the decomposition

$$\boldsymbol{u} = \boldsymbol{u}_0 + \sum_{i=1}^{N} (\boldsymbol{w}_{ir} + \boldsymbol{w}_{i\mathcal{E}}),$$

and by (5.11), (5.12) and (5.13), we conclude that

(5.14)
$$C_0^2 \leq C|\Xi|\chi\eta \left(1 + \log \frac{\delta}{h}\right) \left(1 + \frac{H}{\delta}\right) \left(1 + \log \frac{H}{h}\right).$$

From (5.1) and (5.14), we obtain our main result:

THEOREM 5.1. *The condition number of our overlapping additive two-level Schwarz method is bounded by*

$$\kappa(P_{ad}) \leq C|\Xi|\chi\eta \left(1 + \log \frac{\delta}{h}\right) \left(1 + \frac{H}{\delta}\right) \left(1 + \log \frac{H}{h}\right),$$

where

$$\chi = \max_i \max_{\mathcal{E} \in S_{\mathcal{E}_i}} \chi_{\mathcal{E}}(\delta_i), \ \eta = \max_i \{1 + \beta_i H_i^2/\alpha_i\},$$

and $|\Xi|$ is the maximum number of subdomain edges for any subdomain. The constant C is independent of h_i, H_i, δ_i and the coefficients α_i, β_i.

We can obtain a bound independent of the jumps in the coefficients across the interface with an additional condition:

THEOREM 5.2. *If the mass-dominated subdomains are convex, then the condition number of our overlapping additive two-level Schwarz method is bounded by*

(5.15)
$$\kappa(P_{ad}) \leq C|\Xi|\chi \left(1 + \log \frac{\delta}{h}\right) \left(1 + \frac{H}{\delta}\right) \left(1 + \log \frac{H}{h}\right),$$

where C is independent of h_i, H_i, δ_i and the coefficients α_i, β_i.

Proof. We can improve our result by using a stronger estimate than (4.3a):

$$\|\nabla p\|^2_{L^2(\Omega_i)} \leq C\|\boldsymbol{u}\|^2_{L^2(\Omega_i)};$$

see [14, Theorem 5.2]. Therefore, we can simplify our estimate in (5.5) and then deduce (5.15). ∎

REMARK 5.3. Numerical experiments confirm the estimates of Theorems 5.1 and 5.2: the factor η affects the condition number only when we consider some non-convex decompositions with mass-dominated subdomains ($\alpha_i \leq H_i^2 \beta_i$); see Example 6.2. We also note that the factor $1 + \log \frac{\delta}{h}$ is not relevant: numerical results show that a small overlap gives small condition

ETNA
Kent State University
http://etna.math.kent.edu

numbers for most of the decompositions considered, with the advantage that we obtain local problems in Ω_i' without a significant increase in the size, compared with the local solvers over Ω_i.

REMARK 5.4. For both mass and curl-dominated cases, we can use the inverse inequality in (5.5) to obtain the bound

$$C_0^2 \leq C|\Xi|\chi \left(\frac{\delta}{h}\right)^2 \left(1+\log\frac{\delta}{h}\right)\left(1+\frac{H}{\delta}\right)^3\left(1+\log\frac{H}{h}\right)$$

that is independent of the coefficients α_i and β_i, for general John subdomains. In our experiments with a small overlap δ/h, we have not observed a cubic growth with H/δ, but at times we have seen a quadratic dependence, related to the mass-dominated cases.

REMARK 5.5. For problems in three dimensions, working with irregular subdomains is more challenging. To the best of my knowledge, all previous analyses for the condition number of domain decomposition methods are for convex polyhedral subdomains; e.g., [13, 27, 34]. The main question is how to obtain cutoff functions for the faces and the edges, and a bound for $|I^h\theta_{\mathcal{F}}^{\delta}p|^2_{H^1(\Omega_i)}$ and $|I^h\theta_{\mathcal{E}}^{\delta}p|^2_{H^1(\Omega_i)}$ for irregular subdomains, such as those generated by mesh partitioners. The energy of the edge function grows in proportion to the number of points on the edge, so irregular edges should be treated differently and we need an assumption on the number of nodes in relation to the length of the edge. The energy of the face functions could also be large if there are many edge nodes; see [33]. Some ongoing work is being developed in order to create more tools to handle irregular subdomains in 3D. Recently, in [11], new tools are developed for more general subdomains and a BDDC deluxe method, where the faces are assumed to be only star-shaped polygons. We also note that in [19] a construction for a coarse space in $H(\mathrm{curl})$ is introduced for irregular subdomains and unstructured meshes. For an AMG method, numerical experiments show a linear rate of convergence.

6. Numerical experiments. Numerical examples are presented in this section to confirm the bound of Theorems 5.1 and 5.2 for three different types of subdomains shown in Figure 6.1, for which we consider triangular linear edge elements. Type 1 subdomains have a square geometry, Type 2 subdomains include boundaries with a "sawtooth" shape, and for Type 3 we use equilateral triangles with edges that are part straight, part fractal. Our choices of subdomain geometries are similar to those of [9, Section 5]. See also [10, Section 6.1] for implementation details.

Some numerical results for an overlapping Schwarz method with square edge elements are presented in [10, Section 6] without a theoretical bound. Here we include similar experiments and have provided an analysis. We notice that our condition numbers, in general, are smaller than those obtained in [10]. For purposes of comparison, we also present results for multiplicative and hybrid Schwarz algorithms. We thus also consider the operators

$$P_{mu} = I - E_{mu},$$

with

$$E_{mu} = (I-P_N)(I-P_{N-1})\cdots(I-P_0),$$

and

$$P_{hy1} = I - (I-P_0)(I-\sum_{i=1}^{N} P_i)(I-P_0),$$

where the operators P_i are defined at the beginning of Section 5.

ETNA
Kent State University
http://etna.math.kent.edu

For Type 1 and 2 subdomains, the ratio H/h is increased by a factor of 2 with each additional level of mesh refinement. At the $i-$th ($i \geq 0$) level of refinement for Type 3 subdomains, $H/h = (H/H_f)3^{i+1}$, where $H/H_f = 5$ is fixed. We note that the fractal segment lengths grow by a factor of $4/3$ with each mesh refinement whereas the straight line segments remain constant. For each refinement of Type 3 subdomains, every element edge on the fractal part of the boundary is first divided into three shorter edges of $1/3$ the length. The middle of these edges is then replaced by two other edges with which it forms an equilateral triangle.

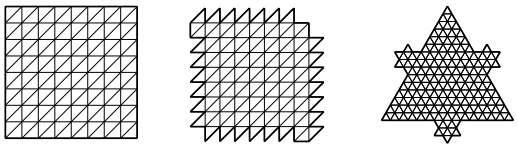

FIG. 6.1. *Type 1, 2 and 3 subdomains used in the numerical examples.*

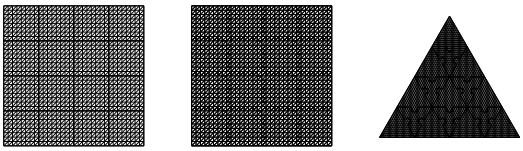

FIG. 6.2. *Type 1, 2 and 3 Domain Decompositions used in numerical examples for* $N = 16$.

We notice that the numerical experiments for our algorithm show an improvement in the iteration count and the condition number estimates, compared to an iterative substructuring method presented in [10]. Nevertheless, a BDDC algorithm with deluxe scaling considered in [5] gives a further significant improvement in the iteration counts and estimates. We note that the overlapping Schwarz method can be used for problems for which only the fully assembled matrix is available, while the BDDC and FETI methods require subdomain matrices corresponding to subdomains problems with natural boundary conditions.

To solve the resulting linear systems, we use a preconditioned conjugate gradient method and random right-hand sides, to a relative residual tolerance of 10^{-8}. The number of iterations and condition number estimates (in parenthesis) are reported for each of the experiments. These estimates are obtained as in [23, Section 4.4]; see also [25, Section 6.7].

EXAMPLE 6.1. We verify the scalability of the algorithm for Type 1 and 2 subdomains over the unit square. As shown in Table 6.1, it is clear that the condition number is independent of the number of subdomains.

EXAMPLE 6.2. This example is used to confirm the factor $(1 + H/\delta)$ in the condition number estimate. For Type 1 and 2 subdomains we use $H/h = 100$ and for Type 3 subdomains, $H/h = 135$, with $N = 16$ in all the cases. Results are shown in Table 6.2. We notice that in these examples the growth is linear, as expected. We also consider the decomposition shown in Figure 6.3. Results are presented in Table 6.3. In this case, for large values of β we observe a quadratic dependence on H/δ, but the condition numbers are in fact quite small; see Figure 6.4.

ETNA
Kent State University
http://etna.math.kent.edu

TABLE 6.1
Results for Type 1 and 2 subdomains, where the unit square is decomposed into N subdomains, with $H/h = 4$, $H/\delta = 4$, $\alpha_i = 1$ and $\beta_i = \beta$.

Type	N	$\beta = 10^{-3}$	$\beta = 1$	$\beta = 10^{3}$
1	64	26(5.7)	22(5.9)	18(4.8)
	256	26(5.7)	23(5.8)	20(5.2)
	576	27(5.8)	24(5.8)	21(5.5)
	784	27(5.8)	24(5.9)	21(5.5)
	1024	27(5.8)	24(5.9)	21(5.5)
2	64	26(6.3)	24(6.2)	18(5.2)
	256	30(7.2)	26(7.3)	20(5.3)
	576	31(7.5)	28(7.6)	21(5.5)
	784	31(7.6)	28(7.7)	21(6.0)
	1024	31(7.7)	28(7.8)	22(6.4)

TABLE 6.2
Results for Type 1, 2 and 3 subdomains with 16 subdomains, $\alpha_i = 1$ and $\beta_i = \beta$. For Type 1 and 2 subdomains, $H/h = 100$; for Type 3, $H/h = 135$. See also Figure 6.4.

Type	H/δ	$\beta = 10^{-5}$	$\beta = 10^{-3}$	$\beta = 1$	$\beta = 10^{3}$	$\beta = 10^{5}$
1	10	31(9.8)	30(9.8)	26(9.9)	19(5.5)	12(4.0)
	20	39(17.8)	37(17.8)	35(17.6)	22(7.9)	13(4.1)
	25	41(21.4)	40(22.6)	38(21.1)	24(8.8)	13(4.1)
	50	60(41.1)	54(40.8)	52(40.7)	30(14.6)	14(4.3)
2	10	30(10.3)	30(10.2)	27(10.4)	21(6.7)	13(4.5)
	20	38(17.0)	38(17.0)	34(17.1)	23(7.6)	14(4.4)
	25	40(19.7)	40(19.7)	38(19.6)	24(9.1)	13(5.1)
	50	54(35.5)	54(34.5)	49(34.1)	29(13.4)	15(5.1)
3	15	49(32.5)	45(33.3)	40(31.9)	26(12.1)	16(5.9)
	27	60(62.5)	56(64.7)	52(57.6)	31(20.1)	16(6.3)
	45	80(117)	73(121)	67(111)	37(31.0)	17(7.4)
	67.5	99(175)	92(185)	81(203)	42(56.0)	18(9.7)

TABLE 6.3
Results for domain decomposition shown in Figure 6.3, with 12 subdomains, $H/h = 96$, $\alpha_i = 1$ and $\beta_i = \beta$. See also Figures 6.3 and 6.4.

H/δ	$\beta = 10^{-5}$	$\beta = 10^{-3}$	$\beta = 1$	$\beta = 10^{3}$	$\beta = 10^{5}$
24	58(45.2)	43(23.1)	55(50.9)	23(7.1)	15(4.3)
32	68(58.2)	47(28.8)	60(83.5)	24(9.0)	15(4.2)
48	85(92.0)	58(47.0)	72(141)	28(14.1)	16(4.5)
96	121(190)	79(99.5)	96(206)	36(39.4)	19(7.3)

EXAMPLE 6.3. This example is used to study the behavior of our algorithm for increasing values of H/h. We present two experiments. First, we use Type 1, 2 and 3 subdomains with constant coefficients, $N = 16$ and $H/\delta = 4$; see Table 6.4. Second, we consider a Type 4 decomposition, similar to Type 2 subdomains but with non-constant coefficients, arranged in a "checkerboard" pattern, using alternating values of 10^{-3} and 10^{3} for α_i and β_i; results are

ETNA
Kent State University
http://etna.math.kent.edu

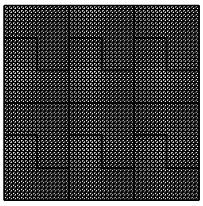

FIG. 6.3. *L-shaped domain decomposition used in Example 6.2. See also Figure 6.4 and Table 6.3.*

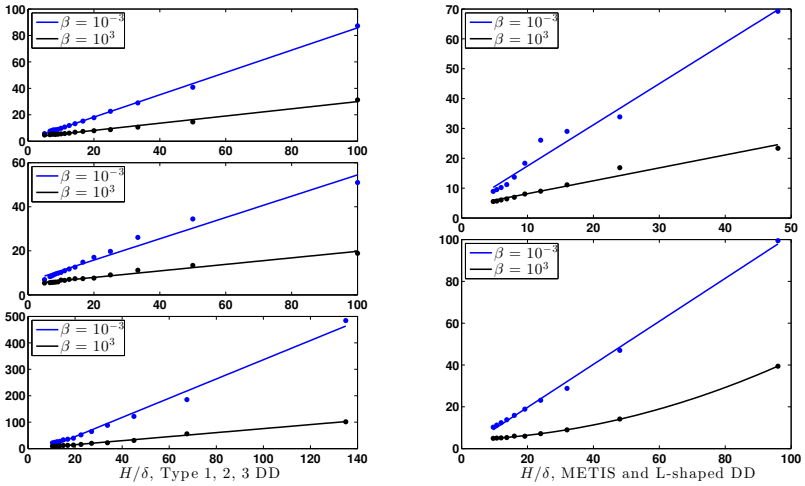

FIG. 6.4. *(Left) Least-squares fit to a linear polynomial in H/δ for data in Table 6.2 for $\beta = 10^{-3}$ and $\beta = 10^{3}$. (Right) Least-squares fit to a polynomial in H/δ for a METIS and a L-shaped domain decomposition; see data in Table 6.3.*

shown in Table 6.5. We note that in these cases the condition number is not sensitive to the mesh parameter H/h.

EXAMPLE 6.4. This example is used to confirm that the estimate is independent of the material property values in the subdomains. Insensitivity to jumps in material properties is evident in Table 6.6. For the first set of experiments, the subdomains along the diagonal have $\alpha_i = \alpha$ and $\beta_i = \beta$, while the remaining subdomains have $\alpha_i = 1$ and $\beta_i = 1$. We also include results with random coefficients, where we generate random numbers $r_{i1}, r_{i2} \in [-3, 3]$ with a uniform distribution, and assign different values of $\alpha_i = 10^{r_{i1}}$, $\beta_i = 10^{r_{i2}}$ for all the elements inside each subdomain Ω_i.

EXAMPLE 6.5. This example is used to confirm that the condition number estimate does not require all subdomain edges to be of comparable length. Here, the smaller subdomains shown in Figure 6.5 have only 6 elements, while the mesh parameter H/h is increased for the larger surrounding subdomains. We use $N = 16$ and $H/\delta = 4$. The results are shown in Table 6.7.

EXAMPLE 6.6. This example is used to demonstrate that the performance of the algorithm need not diminish significantly when a mesh partitioner is used to decompose the mesh. Example mesh decompositions for $N = 16$, $N = 64$ and $N = 144$, shown in Figure 6.6,

ETNA
Kent State University
http://etna.math.kent.edu

TABLE 6.4
Results for the unit square decomposed into 16 subdomains, with $H/\delta = 4$, $\alpha_i = 1$, $\beta_i = \beta$.

Type	H/h	$\beta = 10^{-3}$	$\beta = 1$	$\beta = 10^{3}$
1	16	23(5.5)	21(5.6)	17(5.0)
	32	23(5.5)	21(5.5)	17(4.8)
	64	23(5.3)	22(5.4)	17(4.6)
	128	23(5.4)	22(5.2)	18(4.7)
2	16	24(6.3)	23(5.7)	17(5.1)
	32	25(6.8)	23(5.9)	18(5.1)
	64	25(6.5)	22(5.6)	18(5.1)
	128	25(6.7)	23(6.1)	18(5.1)
3	15	28(8.2)	26(8.0)	20(7.1)
	45	28(8.0)	26(8.0)	21(7.1)
	135	28(8.0)	26(8.0)	22(7.2)

TABLE 6.5
Results for the unit square decomposed into N Type 2 subdomains, with $H/\delta = 4$ and the values α_i and β_i alternating for adjacent subdomains, taking the values 10^{-3} and 10^{3} in a checkerboard configuration.

H/h	$N = 25$	$N = 49$
16	24(7.4)	26(8.7)
32	25(5.9)	26(7.0)
64	24(5.3)	25(5.1)
128	24(5.5)	25(5.6)

were obtained using the graph partitioning software METIS, see [16]. Results are shown in Table 6.8.

EXAMPLE 6.7. We present some results for Type 1 subdomains with the multiplicative and hybrid operators, see [31, Section 2.2]. We use GMRES [26] to solve the associated linear system in the case of the non-symmetric operator P_{mu}. Experimental results show that the symmetrized multiplicative Schwarz method ($P_{mu}^{sym} = I - E_{mu}^{*}E_{mu}$) does not offer a significant advantage. See results in Table 6.9. The multiplicative method improves considerably the number of iterations and the hybrid method behaves slightly better than the additive operator.

EXAMPLE 6.8. This example is used to compare the behavior of our algorithm when the matrix

$$B = \begin{bmatrix} b_{11} & b_{12} \\ b_{12} & b_{22} \end{bmatrix}$$

in (1.1) is not a constant multiple of the identity. We note that our theory does not cover these cases. First we study the variation in the condition number as a function of the entries of B. For this purpose, we consider Type 1 subdomains, with $N = 64$, $H/h = 8$, $H/\delta = 4$, $\alpha = 1$; see Figure 6.7. In general, the condition number slightly increases when there is a big difference between b_{11} and b_{22}, but does not vary in the extreme cases. We also notice a growth in the condition number as the number of subdomains increases. Hence, in this case our coarse space is not satisfactory and the algorithm is not scalable. Nevertheless, it increases logarithmically, and numerical experiments show that the condition number does not deteriorates significantly, see Figure 6.8.

ETNA
Kent State University
http://etna.math.kent.edu

TABLE 6.6
Results for the unit square decomposed into 256 subdomains, with $H/\delta = 8$, $H/h = 16$. The subdomains along the diagonal have $\alpha_i = \alpha$ and $\beta_i = \beta$, while the remaining subdomains have $\alpha_i = 1$ and $\beta_i = 1$.

α	β	Type 1	Type 2
10^{-3}	10^{-3}	31(11.2)	31(10.7)
10^{-3}	1	28(8.1)	27(7.7)
10^{-3}	10^{3}	29(8.8)	28(8.0)
1	10^{-3}	27(9.7)	27(9.9)
1	1	27(8.4)	25(7.8)
1	10^{3}	31(10.8)	27(8.3)
10^{3}	10^{-3}	27(9.6)	27(9.9)
10^{3}	1	27(8.4)	26(7.8)
10^{3}	10^{3}	34(11.1)	26(8.3)
α_{r_1}	β_{r_1}	30(9.1)	27(8.3)
α_{r_2}	β_{r_2}	29(8.2)	28(8.4)
α_{r_3}	β_{r_3}	29(8.1)	27(8.3)
α_{r_4}	β_{r_4}	30(9.1)	27(7.9)
α_{r_5}	β_{r_5}	29(9.1)	27(7.9)

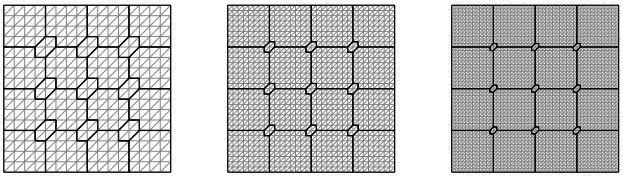

FIG. 6.5. *Example decompositions ($H/h = 4$, $H/h = 8$ and $H/h = 12$) used in Example 6.5. See also Table 6.7.*

TABLE 6.7
Results for the unit square decomposed into 16 large and 9 small subdomains, with $H/\delta = 4$, $\alpha_i = 1$, $\beta_i = \beta$. See also Figure 6.5.

H/h	$\beta = 10^{-3}$	$\beta = 1$	$\beta = 10^{3}$
8	26(6.8)	24(7.0)	19(6.1)
16	27(7.6)	25(7.0)	20(6.1)
32	28(8.3)	25(7.1)	20(6.8)
64	27(8.3)	25(7.0)	20(6.5)
128	27(8.1)	25(7.2)	21(6.2)

EXAMPLE 6.9. This example is used to compare the behavior of our algorithm when there are discontinuous coefficients inside each substructure. Each subdomain is divided in two subregions: in the interior we impose $\alpha = \beta = 1$, and in the second region the coefficients are assigned randomly as in Example 6.4, and then these values are used for all the experiments; see Figure 6.9, Table 6.10 and Table 6.11. For this particular discontinuity pattern, results are similar for any set of random numbers. We note that our theory does not cover these cases. However, our algorithm works well even though there are discontinuities inside each subdomain. A second set of experiments is presented in Table 6.12. Here, each coefficient has

ETNA
Kent State University
http://etna.math.kent.edu

TABLE 6.8
Comparison of results for Type 1 subdomains and subdomains generated by METIS. Material properties are homogeneous with $\alpha_i = 1$, $\beta_i = \beta$. For Type 1 subdomains, $H/h = 8$. For subdomains generated by METIS, see Figure 6.6.

Type	N	$\beta = 10^{-3}$	$\beta = 1$	$\beta = 10^{3}$
1	16	23(5.4)	21(5.5)	16(5.0)
	64	24(5.6)	22(5.4)	19(4.7)
	144	24(5.6)	22(5.5)	19(4.9)
	256	24(5.5)	23(5.5)	20(5.1)
	400	24(5.5)	23(5.5)	21(5.2)
METIS	16	27(7.1)	23(6.8)	19(5.3)
	64	33(8.8)	29(8.8)	23(5.8)
	144	35(11.4)	31(10.9)	25(7.3)
	256	36(12.2)	31(12.0)	26(7.8)
	400	38(11.2)	33(11.1)	27(8.7)

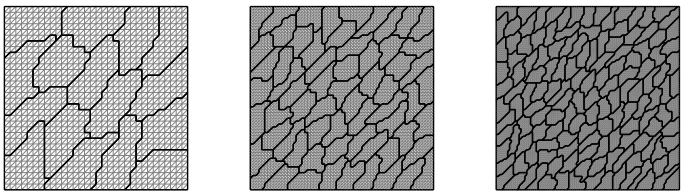

FIG. 6.6. *Decomposition used in Example 6.6, for $N = 16$, $N = 64$ and $N = 144$, obtained with the software METIS.*

TABLE 6.9
Results for Type 1 subdomains, where the unit square is decomposed into N subdomains, with $H/h = 4$, $H/\delta = 4$, $\alpha_i = 1$ and $\beta_i = \beta$.

β	N	P_{ad}	P_{hy}	P_{mu}
10^{3}	144	20(5.0)	18(4.5)	4
	400	21(5.4)	19(5.1)	5
	784	21(5.5)	19(5.5)	5
	1024	21(5.5)	19(5.6)	5
1	144	23(5.8)	22(5.3)	8
	400	23(5.8)	22(5.2)	9
	784	24(5.9)	22(5.2)	9
	1024	24(5.9)	22(5.3)	9
10^{-3}	144	26(5.7)	25(4.9)	12
	400	26(5.8)	25(4.9)	12
	784	27(5.8)	25(5.0)	12
	1024	27(5.8)	25(5.0)	12

four different values for each quarter of the subdomain, assigned randomly for each test; see Figure 6.10. Experimental results show that the condition number deteriorates when we have discontinuities only for β_i, as shown in Table 6.12.

ETNA
Kent State University
http://etna.math.kent.edu

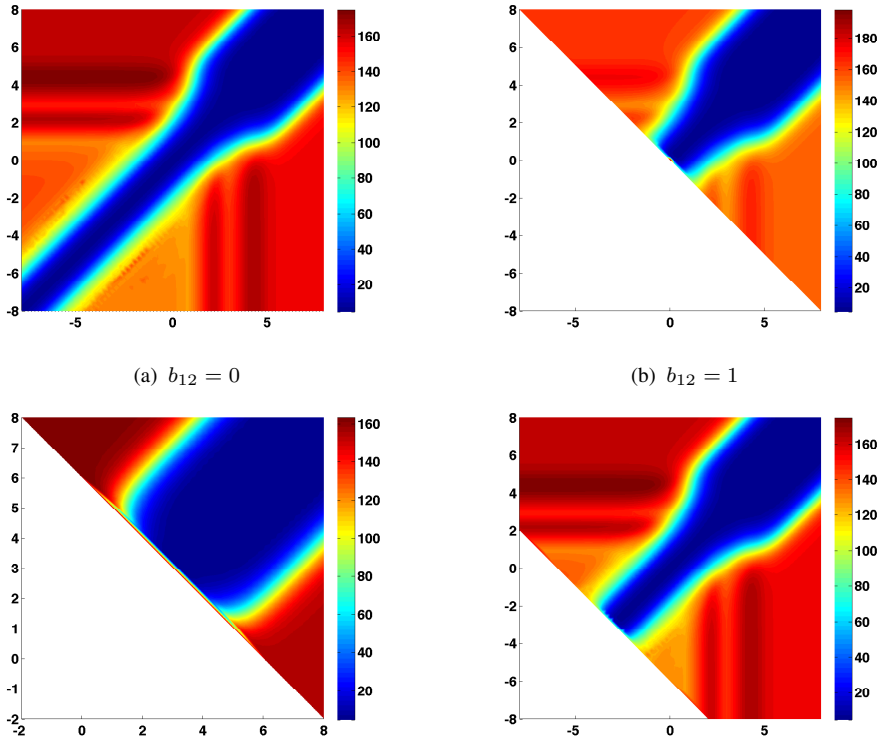

(a) $b_{12} = 0$ (b) $b_{12} = 1$

(c) $b_{12} = 10^{-3}$ (d) $b_{12} = 10^{3}$

FIG. 6.7. *Condition number for different values of* $\log b_{11}$ *(x-axis) and* $\log b_{22}$ *(y-axis).*

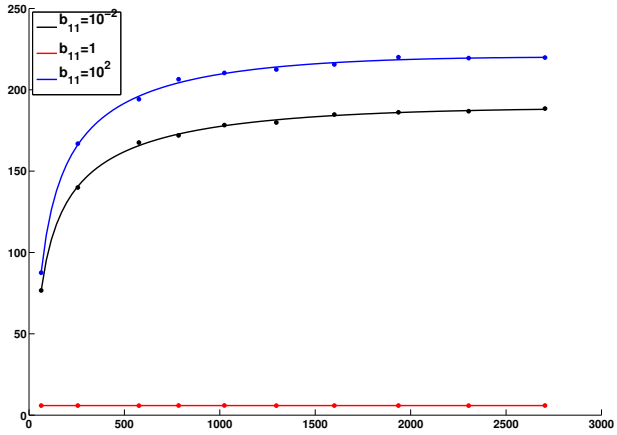

FIG. 6.8. *Condition number as a function of the number of subdomains, for Type 1 subdomains with* $H/h = 4$, $H/\delta = 4$, $\alpha = 1$, $b_{22} = 1$, $b_{12} = b_{21} = 0$.

ETNA
Kent State University
http://etna.math.kent.edu

TABLE 6.10

Results for the unit square decomposed into 64 *subdomains, with* $H/\delta = 8$ *for Type 1 and 2,* $H/\delta = 15$ *for Type 3,* α_i *and* β_i *discontinuous inside each subdomain, as shown in Figure 6.9, where the width of the band is* $1/4$ *of the subdomain diameter.*

Type	H/h	$\alpha = 1$, β_i disc.	$\beta = 1$, α_i disc.	α_i, β_i disc.
1	16	29(9.3)	29(7.3)	30(8.4)
	24	30(9.4)	29(7.4)	31(8.8)
	32	30(9.5)	29(7.5)	31(9.1)
2	16	29(9.2)	28(7.2)	29(9.1)
	24	30(9.5)	28(7.5)	30(10.1)
	32	30(9.7)	29(7.7)	31(10.9)
3	15	32(21.0)	45(26.0)	30(13.2)
	45	33(23.0)	44(27.8)	30(14.7)
	135	33(24.4)	45(28.7)	32(15.1)

TABLE 6.11

Results for the unit square decomposed into 16 *subdomains, with* $H/h = 48$ *for Type 1 and 2,* $H/\delta = 45$ *for Type 3,* α_i *and* β_i *discontinuous inside each subdomain, as shown in Figure 6.9, where the width of the band is* $1/4$ *of the subdomain diameter.*

Type	H/δ	$\alpha = 1$, β_i disc.	$\beta = 1$, α_i disc.	α_i, β_i disc.
1	3	22(5.2)	24(5.1)	23(5.4)
	6	25(6.2)	26(6.3)	27(6.9)
	24	37(17.7)	42(18.1)	38(16.7)
2	3	23(5.4)	24(5.4)	24(5.4)
	6	26(6.9)	27(6.8)	27(7.0)
	24	36(18.7)	40(16.1)	39(16.4)
3	5	27(8.7)	28(8.4)	25(6.4)
	15	32(22.7)	42(28.0)	30(14.2)
	22.5	35(25.9)	52(42.2)	33(18.0)

TABLE 6.12

Results for the unit square decomposed into 16 *Type 1 subdomains, with* $H/h = 16$, $H/\delta = 8$, α_i *and* β_i *discontinuous inside each* Ω_i *and on its interface* Γ_i*, as shown in Figure 6.10.*

$\alpha = 1$, β_i disc.	$\beta = 1$, α_i disc.	α_i, β_i disc.
45(63)	35(14)	56(167)
47(34)	34(14)	45(47)
54(61)	35(14)	45(50)
42(39)	36(15)	54(217)
46(107)	34(14)	46(42)

Acknowledgment. The author would like to thank his advisor, Prof. Olof Widlund, for his guidance and suggestions during the work on this article.

REFERENCES

[1] R. BECK, R. HIPTMAIR, R. H. W. HOPPE, AND B. WOHLMUTH, *Residual based a posteriori error estimators for eddy current computation*, M2AN Math. Model. Numer. Anal., 34 (2000), pp. 159–182.

ETNA
Kent State University
http://etna.math.kent.edu

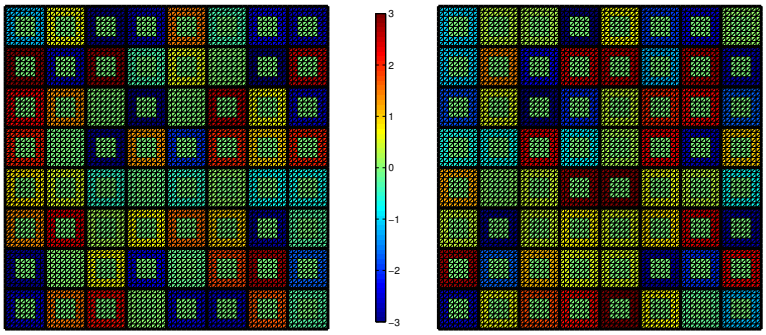

FIG. 6.9. *Coefficient distribution for α (left) and β (right) with Type 1 subdomains used in example 6.9 for $N = 64$. The coefficients were obtained randomly, and then fixed for all the experiments. They vary from 10^{-3} (blue) to 10^{3} (red). See Table 6.10.*

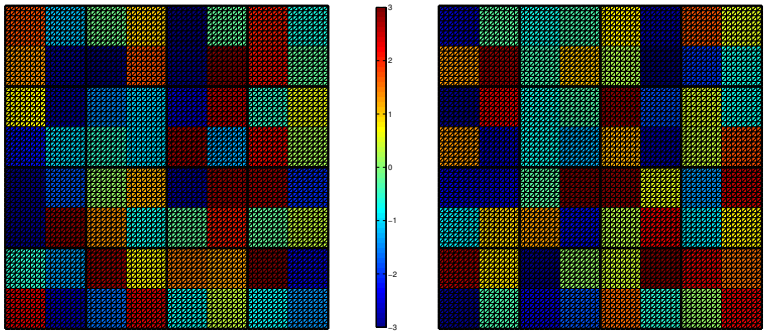

FIG. 6.10. *Coefficient distribution for α (left) and β (right) with Type 1 subdomains used in example 6.9 for $N = 16$. The coefficients vary randomly over the 16 subdomains, from 10^{-3} (blue) to 10^{3} (red). See Table 6.12.*

[2] B. BOJARSKI, *Remarks on Sobolev imbedding inequalities*, in Complex analysis, Joensuu 1987, I. Laine, S. Rickman, and T. Sorvali, eds., Proceedings of Thirteenth Rolf Nevanlinna Colloquium held at the University of Joensuu, 1987, Lecture Notes in Mathematics, 1351, Springer, Berlin, 1988, pp. 52–68.
[3] A. BOSSAVIT, *Discretization of electromagnetic problems: the "generalized finite differences" approach*, in Handbook of Numerical Analysis, Vol. XIII, W. H. A. Schilders and E. J. W. ter Maten, eds., Handb. Numer. Anal., XIII, North-Holland, Amsterdam, 2005, pp. 105–197.
[4] S. M. BUCKLEY AND P. KOSKELA, *Sobolev-Poincaré implies John*, Math. Res. Lett., 2 (1995), pp. 577–593.
[5] J. G. CALVO, *A BDDC algorithm with deluxe scaling for H(curl) in two dimensions with irregular subdomains*, Math. Comp., to appear, 2015.
[6] E. T. CHUNG AND H. H. KIM, *A deluxe FETI-DP algorithm for a hybrid staggered discontinuous Galerkin method for* $\mathrm{H}(\mathrm{curl})$*-elliptic problems*, Internat. J. Numer. Methods Engrg., 98 (2014), pp. 1–23.
[7] C. R. DOHRMANN, A. KLAWONN, AND O. B. WIDLUND, *Domain decomposition for less regular subdomains: overlapping Schwarz in two dimensions*, SIAM J. Numer. Anal., 46 (2008), pp. 2153–2168.
[8] C. R. DOHRMANN AND O. B. WIDLUND, *An overlapping Schwarz algorithm for almost incompressible elasticity*, SIAM J. Numer. Anal., 47 (2009), pp. 2897–2923.
[9] ———, *An alternative coarse space for irregular subdomains and an overlapping Schwarz algorithm for*

ETNA
Kent State University
http://etna.math.kent.edu

scalar elliptic problems in the plane, SIAM J. Numer. Anal., 50 (2012), pp. 2522–2537.

[10] ———, *An iterative substructuring algorithm for two-dimensional problems in* $H(\mathrm{curl})$, SIAM J. Numer. Anal., 50 (2012), pp. 1004–1028.

[11] ———, *A BDDC algorithm with deluxe scaling for three-dimensional* $H(curl)$ *problems*, Comm. Pure Appl. Math, in print, doi:10.1002/cpa.21574.

[12] H. FEDERER AND W. H. FLEMING, *Normal and integral currents*, Ann. of Math. (2), 72 (1960), pp. 458–520.

[13] R. HIPTMAIR AND A. TOSELLI, *Overlapping and multilevel Schwarz methods for vector valued elliptic problems in three dimensions*, in Parallel Solution of Partial Differential Equations, P. Bjørstad and M. Luskin, eds., IMA Vol. Math. Appl., 120, Springer, New York, 2000, pp. 181–208.

[14] R. HIPTMAIR AND J. XU, *Nodal auxiliary space preconditioning in* $\mathbf{H}(\mathbf{curl})$ *and* $\mathbf{H}(\mathrm{div})$ *spaces*, SIAM J. Numer. Anal., 45 (2007), pp. 2483–2509.

[15] F. JOHN, *Rotation and strain*, Comm. Pure Appl. Math., 14 (1961), pp. 391–413.

[16] G. KARYPIS AND V. KUMAR, *A fast and high quality multilevel scheme for partitioning irregular graphs*, SIAM J. Sci. Comput., 20 (1998), pp. 359–392.

[17] A. KLAWONN, O. RHEINBACH, AND O. B. WIDLUND, *An analysis of a FETI-DP algorithm on irregular subdomains in the plane*, SIAM J. Numer. Anal., 46 (2008), pp. 2484–2504.

[18] T. V. KOLEV AND P. S. VASSILEVSKI, *Parallel auxiliary space AMG for* $H(\mathrm{curl})$ *problems*, J. Comput. Math., 27 (2009), pp. 604–623.

[19] I. V. LASHUK AND P. S. VASSILEVSKI, *The construction of the coarse de Rham complexes with improved approximation properties*, Comput. Methods Appl. Math., 14 (2014), pp. 257–303.

[20] V. G. MAZ'JA, *Classes of domains and imbedding theorems for functions spaces*, Soviet Math. Dokl., 1 (1960), pp. 882–885.

[21] J.-C. NÉDÉLEC, *Mixed finite elements in* $\mathbf{R}^3$, Numer. Math., 35 (1980), pp. 315–341.

[22] D.-S. OH, *An overlapping Schwarz algorithm for Raviart-Thomas vector fields with discontinuous coefficients*, SIAM J. Numer. Anal., 51 (2013), pp. 297–321.

[23] D. P. O'LEARY AND O. WIDLUND, *Capacitance matrix methods for the Helmholtz equation on general three-dimensional regions*, Math. Comp., 33 (1979), pp. 849–879.

[24] A. QUARTERONI AND A. VALLI, *Numerical Approximation of Partial Differential Equations*, Springer, Berlin, 1994.

[25] Y. SAAD, *Iterative Methods for Sparse Linear Systems*, 2nd ed., SIAM Philadelphia, 2003.

[26] Y. SAAD AND M. H. SCHULTZ, *GMRES: a generalized minimal residual algorithm for solving nonsymmetric linear systems*, SIAM J. Sci. Statist. Comput., 7 (1986), pp. 856–869.

[27] A. TOSELLI, *Overlapping Schwarz methods for Maxwell's equations in three dimensions*, Numer. Math., 86 (2000), pp. 733–752.

[28] ———, *Dual-primal FETI algorithms for edge finite-element approximations in 3D*, IMA J. Numer. Anal., 26 (2006), pp. 96–130.

[29] A. TOSELLI AND A. KLAWONN, *A FETI domain decomposicion method for edge element approximations in two dimensions with discontinuous coefficients*, SIAM J. Numer. Anal., 39 (2002), pp. 932–956.

[30] A. TOSELLI AND X. VASSEUR, *Robust and efficient FETI domain decomposition algorithms for edge element approximations*, COMPEL, 24 (2005), pp. 396–407.

[31] A. TOSELLI AND O. WIDLUND, *Domain Decomposition Methods—Algorithms and Theory*, Springer, Berlin, 2005.

[32] A. TOSELLI, O. B. WIDLUND, AND B. I. WOHLMUTH, *An iterative substructuring method for Maxwell's equations in two dimensions*, Math. Comp., 70 (2001), pp. 935–949.

[33] O. B. WIDLUND, *Accommodating irregular subdomains in domain decomposition theory*, in Domain Decomposition Methods in Science and Engineering XVIII, M. Bercovier, M. J. Gander, R. Kornhuber, and O. B. Widlund, eds., Lecture Notes in Computational Science and Engineering, 70, Springer, Berlin, 2009, pp. 87–98.

[34] B. I. WOHLMUTH, A. TOSELLI, AND O. B. WIDLUND, *An iterative substructuring method for Raviart-Thomas vector fields in three dimensions*, SIAM J. Numer. Anal., 37 (2000), pp. 1657–1676.